

**Hamburg University of Applied Sciences**

**Faculty of Life Sciences**

Master Thesis

Biomedical Engineering

Submitted by Ewald Schmidt



Hamburg

04, September 2020

## Evaluation and Optimisation of a Catheter Simulation for Endovascular Navigation

<b>First Examiner:</b>	Prof. Dr. Anna Rodenhausen	(Hamburg, University of Applied Sciences)
<b>Second Examiner:</b>	Dr. Jan Strehlow	(Bremen, Fraunhofer Institute for Digital Medicine MEVIS)

In Cooperation with the Fraunhofer Institute for Digital Medicine MEVIS

## Preface

In this thesis I will discuss the topic of catheter navigation and focus mainly on the evaluation and optimisation of a new navigation approach called IntelliCath. My first interaction with catheter navigation was in my bachelor thesis, where I worked on the possibility to use auditory display to navigate a catheter inside a patient's vessel system. At that point, my interest for this topic was awakened. It was fascinating to see how challenging the catheter navigation is even in contemporary medicine. While searching for a topic for my master thesis, I was pleased to see that I had an opportunity to "return" to this interesting field of science, although the approach was a different one this time.

Thanks to the support of my supervisor Dr. Jan Strehlow, who always provided guidance and helpful input throughout my time at Fraunhofer MEVIS, I was able to get a deeper understanding of the subject matter. The other students I worked with were always immensely helpful and supportive when it came to little programming difficulties that for some reason I could not solve myself. Sometimes you need a neutral person to take a look at your program. I am incredibly grateful for having the opportunity to work with such competent, supportive and charming people. I want to especially thank Dr. Jan Strehlow, Professor Dr. Anna Rodenhausen and the complete staff at Fraunhofer MEVIS. Surely this thesis would have looked different without you.

## Abstract of this Thesis

Catheter navigation is a key issue of contemporary endovascular intervention. The navigation still requires a high level of training and experience to be successful and nevertheless comes with numerous intricacies like radiation exposure and negative side effects from contrast agents. To overcome the steep learning curve and error susceptibility, as well as other issues, a catheter navigation approach was developed. The alleged solution is to simulate a catheter path, using the patients vessel system as basis, and then compare its curvature to the measured curvature of the actual catheter inside the patient in order to localize its position in the human body.

For this master thesis, the given task is to detect the accuracy of a catheter simulation program and optimise its implemented parameters in order to improve the catheter simulation. In order to do this, a segmentation network is developed, which extracts and processes the image data needed for the simulation. Subsequently, an evaluation network is developed to determine the accuracy of a set simulation module by comparing the catheter simulation to the real catheter that moves through the vessel. Finally, the parameters embedded into the simulation algorithm are strategically changed in order to lower the error value of the simulation.

The aim is to determine the accuracy of the simulation module in relation to reality and thus assess its suitability for use in the medical environment. If the simulation approach is proven to be close to reality, the optimal parameter setting must be modified with regards to the computational strain and accuracy.

## Table of contents

Preface.....	I
Abstract of this Thesis .....	II
1 Current State of Catheter Navigation.....	1
1.1 IntelliCath Catheter Navigation Approach.....	2
2 Aim of the Thesis .....	4
3 Fundamentals of Image Processing .....	5
3.1 Segmentation Algorithms .....	5
3.1.1 Interval Threshold.....	5
3.1.2 Region Growing .....	5
3.2 Edge Detection using Sobel.....	6
3.3 Binary Morphological Operations .....	9
3.4 Euclidean Distance.....	12
3.5 B-Spline Interpolation.....	12
3.6 Catheter Simulation.....	13
3.6.1 Newton Optimiser.....	14
3.6.2 Cost Function and Curvature Calculation.....	14
4 General Evaluation Approach of the Catheter Simulation.....	16
4.1 MeVisLab as a Platform for Medical Imaging.....	16
4.2 Methodology of this Thesis .....	18
5 Image Data Processing.....	19
5.1 Candle Holder .....	20
5.2 Physiological Vessel Phantoms .....	21
5.3 Camera Recordings .....	23
5.4 Imaging Data Segmentation (Candle Holder) .....	24
5.4.1 Catheter Segmentation.....	24
5.4.2 Catheter Skeletonization and Sampling.....	27
5.4.3 Inner Vessel Segmentation.....	29
5.4.4 Adding missing Vessel Connections .....	31
5.4.5 Graph Manipulation.....	31
5.4.6 Graph Root detection and Sampling .....	34
5.4.7 Other Phantoms .....	34
5.4.8 Final Data Structure .....	37

5.5 Overlapping and Cropping Catheter Paths for Evaluation .....	38
6 Evaluation and Optimisation of the Simulation Approach.....	41
6.1 Simulation Algorithm and Simulation Parameters .....	41
6.2 Additional Influence Factors analysed in this Thesis .....	44
6.2.1 Sampling Distance in Relation to Curvature .....	44
6.2.2 Influence of Mechanical Forces on the Curvature of the Catheter .....	44
6.3 Euclidean Distance Calculation .....	45
6.4 Evaluation Network .....	47
6.5 Iterations .....	47
7 Results of the Optimisation .....	48
7.1 Physiological Vessel Phantoms .....	52
7.2 Candle Holder Phantom .....	54
7.3 Other Analysed Parameters.....	56
8 Discussion.....	58
9 Conclusion .....	62
10 Outlook .....	64
Bibliography .....	III
List of Figures .....	V
List of Graphs.....	VII
List of Tables.....	VIII
Appendix.....	X

# 1 Current State of Catheter Navigation

Catheters have been used since ancient times “for more than 3500 years, urinary catheters have been used to drain the bladder when it fails to empty” (Feneley, Hopley, & Wells, 2015, p. 459). In contemporary medicine, catheters are frequently used for therapeutic and diagnostic purposes due to their immense applicability. In this thesis the emphasize lies on catheters which are used inside the vascular system of a patient, the so-called endovascular catheters and specifically on their navigation within the vascular system. “Endovascular therapy has continuously evolved since it was first described in 1904. It was first used as a technique to inject particles to follow the flow into vascular lesions” (Richling, 2006, p. S3-30). As conducted by the Society of Vascular Surgery, which published a study showing the increase of endovascular procedures in the United States between 1980-2000, the increase in “catheter based endovascular interventions (here angioplasty, noncoronary stent placement, and intraluminal thrombolytic therapy, including carotid stenting)” (see Anderon, et al., 2004, p. 1201) increased from “0.1 procedures per 100,000 population to 58,3 procedures per 100,000 population” (see Anderon, et al., 2004, p. 1202). This shows the drastic increase in the use of catheters for endovascular procedures. Despite their long presence in the clinical environment and their high applicability and use, contemporary catheter interventions are associated with a variety of difficulties and provide an enormous challenge for angiologists.

“Usually, the endovascular and endocranial navigation of the diagnostic and ablation catheter is guided by fluoroscopy” (Luani, et al., 2019, p. 2). The issues here are that “fluoroscopic procedures (particularly prolonged interventional procedures) may involve high patient radiation doses” (Mahesh, 2001, p. 1033), additionally iodine contrast agents are injected into the patient’s body to increase the visual output of the fluoroscopy. Above that, by looking at the two-dimensional image of the fluoroscopy, the physician must anticipate the three-dimensional position of the catheter within the vessel system and navigate to the desired target area. A high level of experience is required to correctly interpret the two-dimensional images into three-dimensional position data. In addition, high doses of iodine contrast agents are extremely stressful for the kidneys, and radiation exposure is a risk factor for the health of both the patient and the physician. Given the previously mentioned issues contemporary medicine is eager to find a solution that

minimises the previously stated issues. This master thesis focuses on one of these approaches called IntelliCath.

## 1.1 IntelliCath Catheter Navigation Approach

In the following passage the IntelliCath technology is further described, to give the overall framework in which this thesis is settled.

The IntelliCath technology is currently under development at the Fraunhofer MEVIS Institute. Its goal is to improve catheter navigation by providing a three-dimensional navigation system based on imaging data from the patient. The main idea of this project is to use curvature data drawn from the catheter and compare it to curvature data extracted from a computed model of the patient's vascular system. Ideally, by comparing the curvature of each vessel branch of the patient's vessel system with the curvature of the inserted catheter to find similar or equal curvature compositions, it should be possible to determine the catheters position inside the patient.

As mentioned above, the comparison is solely based on curvature data provided from the catheter and the segmented vessel system. The curvature data is acquired from the catheter by using multicore fibres. The previously detected images provided curvature data based on each segmented vessel path. Of course, this approach relies heavily on the correct segmentation of the vessel system as well as accurate predictions concerning the catheter curvature inside the vessel. In the later part initial difficulties arise. To enable the comparison between vessel path and catheter path, the vessel path at first needed to be converted into something resembling a catheter. The first approach was to condense each tubular vessel path to its centre line and then compare each centre line representation with the given catheter path to find the right fit. Ideally, the curvature of the centre line representations will match the curvature of the catheter, indicating where the catheter is located. However, the accuracy of the navigation approach relies heavily on correct assumptions regarding the catheter movement through each given vessel path.

After analysing the data, it appeared that the centre line representation of each vessel path has flaws, because firstly, the way a catheter moves through a vessel is not along a centre line and subsequently, when using the centre line representation, immense curvature values were generated at branches where a vessel separates as seen in figure

1. This happens because the shape of a catheter in a vessel differs drastically from the shape of the centreline in particular at bifurcations.

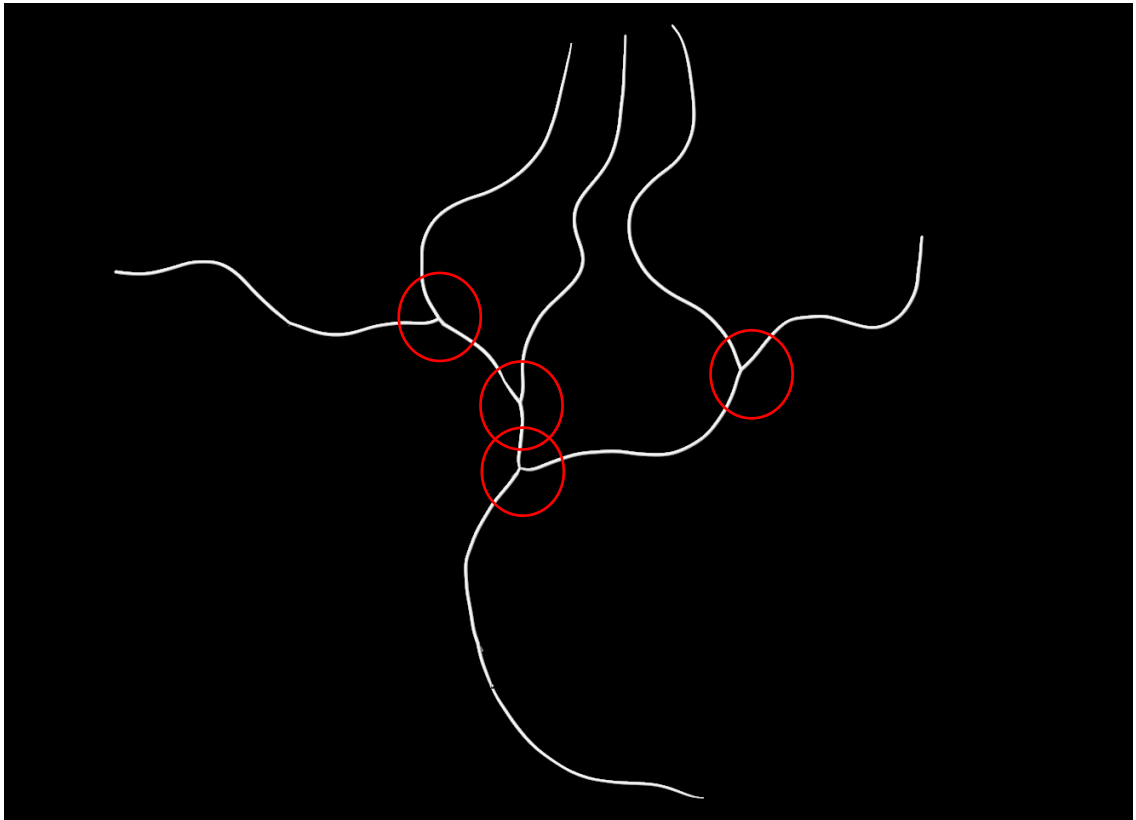


Figure 1: Centre line representation of a vessel system. At the bifurcations (circled in red) it can be observed that the curvature values are high.

To mitigate those difficulties an iterative approach to simulate a catheter inside a vessel was developed. This approach assumes that a catheter moves through a vessel system along a curvature minimising path. The determination of the accuracy of this assumption with regards to reality and optimising the catheter simulation algorithm are the focus points of this master thesis. Sensory data is not used in this thesis, and all extracted information is segmented from multiple sets of imaging data.



## 2 Aim of the Thesis

Before diving into the depths of segmentation, and data evaluation as well as data optimisation, it is important to further concretise the goals of this thesis. The goal can be decomposed into two parts: Evaluation and optimisation.

The first part is dedicated to evaluation. It focuses on evaluating the catheter simulation approach, i.e. how well the curvature minimising approach resembles reality. This is done by comparing multiple simulated and real catheter paths, from different data sets to each other.

Subsequently, if the evaluation comes to the conclusion that a curvature minimising approach is a sufficiently accurate way to represent a catheter path, parameters implemented in the catheter simulation algorithm will be adjusted and optimised to improve the overall result and provide an optimal trade-off between simulation accuracy and computational strain. Several simulated and real catheter paths, from different data sets, are compared consecutively with varying parameter settings, to find the setting that result in the closest approximation to the real catheter path.

At the end, an overall conclusion is drawn, presenting the optimal parameter setting and the closeness to reality of the simulation approach.

## 3 Fundamentals of Image Processing

Fundamentals explain general principles and functionalities of the segmentation approach as well as iterative optimisation, -distance analysis and interpolation methods used in this thesis. Its purpose is to provide a foundation that allows everybody without a deep understanding of these topics to understand the methods and approaches used in this thesis.

### 3.1 Segmentation Algorithms

The chapter segmentation algorithms focuses on different forms of structure and information extraction from image data based on given parameters. This includes the removal of excess information from the imaging data. Segmentation is a focus in this thesis and is described in the following.

#### 3.1.1 Interval Threshold

A threshold is one of the simplest methods for image segmentation. The main idea is to “select a threshold value  $X$ , which then converts a grey value image into a binary image by assigning all grey values below  $X$  to a value of 0 (black/background) and all grey values equal or above  $X$  as 1 (white/foreground)” (see Al-amri, Kalyankar, & Khamtikar, 2010, p. 83). This method is used throughout to filter out parts from the image.

#### 3.1.2 Region Growing

Region growing is another core segmentation method used in this thesis. “Region growing is the process of grouping neighbouring pixels into regions. The process of merging pixels or regions to produce larger regions is usually governed by a homogeneity criterion” (see Ikonomakis, Plataniotis, & Venetsanopolous, 2000, p. 9). In this case, the homogeneity criterion is represented by an upper and lower threshold, which defines by how much the grey value of a voxel can differ from the original seed

grey value, that is selected manually at the beginning, in order to be counted to its neighbourhood. With this knowledge, region growing can be used to select and segment areas within an image that share similar grey values. It is an important tool in this thesis and will be mentioned several times.

### 3.2 Edge Detection using Sobel

Edge detection describes the process of being able to “detect distinct changes in the intensity of an image and recognize them as edges and therefore is fundamental for low-level image processing” (see Sengur, Guo, Ustundag, & Alcin, 2015, p. 235). “Edges are considered as the boundaries between different textures. In figure 2, the general principle of image processing using matrixes is visualised. Here a 3x3 matrix is applied to a random input image.

$$\text{Input Image} = \begin{bmatrix} A_{11} & \cdots & A_{1m} \\ \vdots & \ddots & \vdots \\ A_{n1} & \cdots & A_{nm} \end{bmatrix} = \begin{bmatrix} 0 & 0 & 0 & 0 & 0 \\ 0 & 100 & 120 & 105 & 0 \\ 0 & 200 & 210 & 190 & 0 \\ 0 & 190 & 220 & 230 & 0 \\ 0 & 0 & 0 & 0 & 0 \end{bmatrix}$$

$$\text{Matrix} = \begin{bmatrix} B_{11} & \cdots & B_{1m} \\ \vdots & \ddots & \vdots \\ B_{n1} & \cdots & B_{nm} \end{bmatrix} = \begin{bmatrix} 0 & 0,2 & 0 \\ 0,2 & 0,2 & 0,2 \\ 0 & 0,2 & 0 \end{bmatrix}$$

$$\text{Output Image} = \begin{bmatrix} C_{11} & \cdots & C_{1m} \\ \vdots & \ddots & \vdots \\ C_{n1} & \cdots & C_{nm} \end{bmatrix} = \begin{bmatrix} 0 & 0 & 0 & 0 & 0 \\ 0 & 84 & 107 & 83 & 0 \\ 0 & 140 & 188 & 127 & 0 \\ 0 & 122 & 170 & 128 & 0 \\ 0 & 0 & 0 & 0 & 0 \end{bmatrix}$$

Calculation example for calculating the value marked in red, exemplarily the pixel  $A_{22}$  is replaced by:

$$\begin{aligned}
C_{22} &= B_{21} * A_{21} + B_{12} * A_{12} + B_{23} * A_{23} + B_{32} * A_{32} + B_{22} * A_{22} \\
&= 0 * 0,2 + 0 * 0,2 + 0,2 * 120 + 0,2 * 200 + 0,2 * 100 \\
&= 0 + 0 + 24 + 40 + 20 \\
&= 84
\end{aligned}$$

Figure 2: Filter application in digital image processing.

Differential edge detection approaches, used in this thesis, apply a matrix to each pixel in an input image, transforming its intensity value. The shape of the transformation matrix determines the filter operation. In this thesis, transformation matrixes in edge detection are used to determine the first derivative of each pixel in the input image  $I(x, y)$ , which is a pixel intensity function at location  $(x, y)$ , to then transform these derivatives into a gradient. The edge detection methods used in this thesis are gradient based, which means that “the assumption is that edges are the pixels with a high gradient” (Sengur, Guo, Ustundag, & Alcin, 2015, p. 236). Therefore they work on the assumption that “if one take the derivative of the intensity value across the image and find points where the derivative is maximum, then the edge could be located” (Olufunke & Olusegun, 2009, p. 100). There are many different approaches to edge detection, for example, “Canny, Marr-Hildreth, Sobel, or Prewitt” (see Sengur, Guo, Ustundag, & Alcin, 2015, p. 235). In this thesis the focus is on the edge detection method called Sobel. Edge detection in this thesis is a sufficient method to separate image borders that are blurred by connecting them with other segmentation steps.

Sobel is an edge detection method. Its functionality can be described as “a gradient-based method that looks for strong changes in the first derivative of an image” (Farber, 2011, p. 280), therefore approximating the highest gradient position of an input image in x-and y direction by using the first partial derivative of its intensity function as basis for the calculation.

Using the intensity of each pixel as the basis for the calculation is a reliable source of information and provides sufficient edge detection results. However, the usability of these intensity functions depends on their accuracy, which in terms means that “high-frequency noise creates false edges in the filtered image, so often the image is filtered with a Gaussian filter prior to applying the Sobel filter” (Bakos, 2016, p. 155), as visualised in equation 1.



### 3.3 Binary Morphological Operations

Binary morphological operations like “erosion and dilations are two fundamental morphological operations from which many others are derived” (see Hedberg, 2008, p. 33). They are commonly used in image processing and are a practical tool in this thesis. They are defined by a structural element that is applied to each pixel in an image. Based on the form of the structural element and the morphological operation, the structural element either changes the value of pixels to one (black) or to zero (white) in a binary image.

#### Erosion

Erosion is an operation to modify a “binary image  $I \subset \mathbb{Z}^2$  by means of a structural element  $B \subset \mathbb{Z}^2$ ” (see Hedberg, 2008, p. 33) and is used to “reduce objects in the image” (Sreedhar & Panlal, 2012, p. 36) by moving the structural element  $B$  over every pixel in image  $I$ . In a binary image this means that “if any pixel that encounters the structural element is set to 0, the output pixel is set to 0” (see Sreedhar & Panlal, 2012, p. 36). Erosion can be notated by

$$I \ominus B.$$

Equation 4: Notation for erosion.

This minus sign inside the circle indicates that the number pixels with value 1 in an image in general will be reduced when erosion is applied. An example for erosion is shown in figure 3. This procedure narrows structures as illustrate in figure 3. Erosion is implemented in the skeletonization and closing operation used in this thesis and is “computed only on the original grid” (MeVis Medical Solutions AG [a]) of the input image.

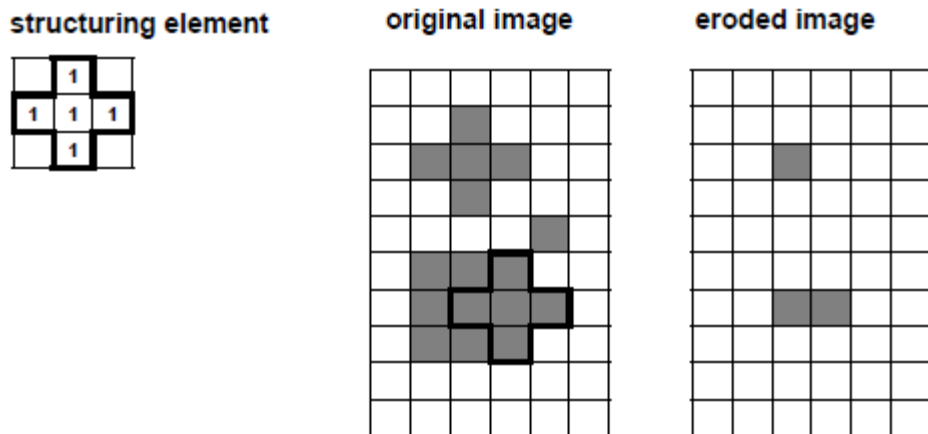


Figure 3: Erosion process visually illustrated. Here, black pixels have the value 1 and white pixels the value 0.

## Dilation

Dilation is a complementary operation compared with erosion. Again, a “binary image  $I \subset \mathbb{Z}^2$  is modified according to a given structural element  $B \subset \mathbb{Z}^2$ ” (see Hedberg, 2008, pp. 34-35). Dilation widens structures and does the opposite of erosion. “In a binary image, if any of the pixels is set to the value 1 it sets the output pixel to 1” (see Sreedhar & Panlal, 2012, p. 36). Dilation can be written as

$$I \oplus B.$$

Equation 5: Notation for dilation.

This indicates that the number of pixels with value 1 in the binary image in general will be increased by dilation. In this thesis, the dilation operation “virtually expands the input image by some voxels so that the structural element can filter all image voxels correctly. The contents of the area added around the input image are filled with the nearest voxel found in the input image” (see MeVis Medical Solutions AG [e]).

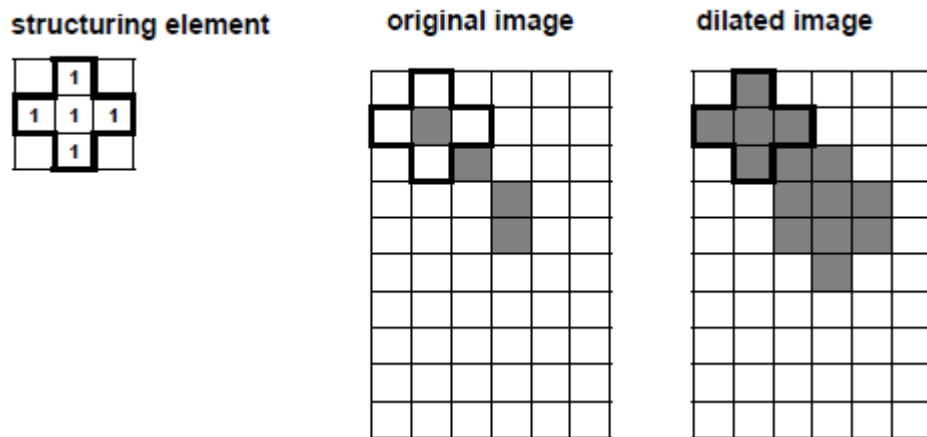


Figure 4: Dilation process visually illustrated.

It is worth mentioning that erosion and dilation in general do not neutralize each other, i.e. in general we do not find

$$(I \ominus B) \oplus B = I \text{ or } (I \oplus B) \ominus B = I.$$

Equation 6: Notion of the irreversibility of erosion and dilation.

## Closing

Closing is a morphological operation that is given by a concatenation of erosion and dilation. "Closing is a dilation followed by an erosion" (Hedberg, 2008, p. 36). First, the dilation operator is used to widen the image and then the erosion operation is applied to narrow the image again. This is done to "reconnect split object" (Hedberg, 2008, p. 36). Closing is mathematically defined as:

$$(I \oplus B) \ominus B.$$

Equation 7: Closing mathematically defined as dilation followed by erosion.

This formula further illustrates that "closing is defined as dilation followed by erosion" (see Hedberg, 2008, p. 36).



### 3.4 Euclidean Distance

In the later part it is discussed how parameters are adjusted and the simulation is evaluated. The basis for this is provided by the Euclidean distance. The Euclidean distance “measures the regular distance between two points in space” (Hossain & Abufardeh, 2019, p. 45). The Euclidean distance can be described as follows: “if  $p$  and  $q$  are points in  $\mathbb{R}^3$ , the Euclidean distance from  $p$  to  $q$  is the number:

$$d(p, q) = \|p - q\|.$$

In fact, since

$$p - q = (p_1 - q_1, p_2 - q_2, p_3 - q_3),$$

expansion of the norm gives the well-known formula” (O'Neill, 2006, p. 44)

$$\|p - q\| = ((p_1 - q_1)^2 + (p_2 - q_2)^2 + \dots + (p_n - q_n)^2)^{1/2}.$$

Equation 8: Euclidean distance calculation for distance between point  $p$  and  $q$  in  $\mathbb{R}^3$ .

### 3.5 B-Spline Interpolation

The Basic-Spline interpolation method, also called B-Spline interpolation, is an interpolation method used in this thesis to calculate “a smooth continuous curve passing through a set of discrete data at certain spatial points” (Hou & Andrews, 1978, p. 508). In this case the interpolate is performed to decrease the sampling distance of a simulated catheter path and therefore increase its number of markers.

“The B-spline interpolate of order  $n$  of a discrete signal  $f \in \mathbb{R}^{\mathbb{Z}}$  is the spline  $\varphi^{(n)}$  of degree  $n$  defined for  $x \in \mathbb{R}$  by

$$\varphi^{(n)}(x) = \sum_{i \in \mathbb{Z}} c_i \beta^{(n)}(x - i),$$

Equation 9 Spline calculation represented as “weighted sum of shifted normalized B-splines of order  $n$ ”.

where the B-spline coefficients  $c = (c_i)_{i \in \mathbb{Z}}$  are uniquely characterized by the interpolating condition” (Briand & Monasse, 2018, p. 101)

$$\varphi^{(n)}(k) = f_k, \forall k \in \mathbb{Z}.$$

Equation 10: Interpolation condition.

“Here,  $\beta^{(n)}$  represents the B-Spline function and  $n$  a non-negative integer” (see Briand & Monasse, 2018, p. 101). The module used in this thesis which applies this interpolation approach, always uses a cubic B-spline interpolation approach ( $n = 3$ ).

### 3.6 Catheter Simulation

This chapter explains the functionality of the catheter simulation module provided in this thesis.

The catheter simulation process starts with inserting a starting value into the simulation. Here it always starts with the centre line of the previously segmented vessel system. Additionally, boundary conditions are included in the simulation, which in this case is the vessel geometry. The vessel geometry limits the simulation in such a way that a catheter simulation outside the vessel is not possible. The simulation then models the catheter as a curvature minimising object. To simulate this, it uses a Newton optimiser, which is explained in chapter 3, subsection 3.6.1, that utilizes a cost function, which is described in chapter 3, subsection 3.6.2, in order to iteratively find a curvature minimising catheter path. Along the simulation process the current optimal path is changed and evaluated throughout each iteration. Each time the optimiser discovers a new optimal catheter path, with a less sum of curvature than the current optimal path, it sets this path as the new optimal catheter path.

### 3.6.1 Newton Optimiser

We consider the path with minimal curvature as a sequence of pixels, where the curvatures over all pixels are minimal. This sequence of pixels represents the calculated catheter path used in this thesis.

The underlying method to determine the curvature minimising path for a simulated catheter is the Newton optimiser. The idea behind the Newton optimiser is, “given a starting point, we construct a quadratic approximation to the objective function that matches the first and second derivative value at that point. We then minimise the approximate (quadratic) function instead of the original objective function” (Chong & Zak, 2001, p. 139). “The vector  $x$  that yields the smallest value of the objective function, is called the minimiser” (see Chong & Zak, 2001, p. 73). This vector is then used as the starting point of the next step. In this thesis this is used to minimise the curvature of the catheter path generated from the vessel systems, which are segmented in this thesis. By evaluating different generated catheter paths for every iteration step, the Newton optimiser can use these evaluation values to generate a quadratic function. The minimum of the quadratic function on the objective function is then used as a new iteration step, where the complete procedure is performed again, as described in chapter3, subsection 3.6.

### 3.6.2 Cost Function and Curvature Calculation

The objective function or cost function in this optimisation approach models the catheter as a non-stiff curvature minimising object that is used to evaluate newly generated catheter paths. Using the centre line representation of the vessel system as a starting point, the optimiser generates multiple new catheter paths with varying shapes. These paths are evaluated with regards to their sum of curvatures. Each evaluation output represents a point on the cost function, which is unknown. These additional evaluation points in the cost function are necessary to perform the Newton optimisation process, as explained previously, i.e. to compute the quadratic approximation. Therefore, the cost function is used to identify the optimal value and thereby find the best new catheter path.

The optimiser minimises the cost-function to find the smallest sum of curvatures a catheter path can have and therefore the optimal curvature minimising catheter path.

The curvature is calculated using the Menger curvature. The method makes use of three non collinear points ( $z_1, z_2, z_3$ ) to calculate their curvature. The Menger curvature for three non collinear points is calculated by:

$$c(z_1, z_2, z_3)^2 = \left( \frac{4S(z_1, z_2, z_3)}{|z_1 - z_2| |z_2 - z_3| |z_3 - z_1|} \right)^2,$$

Equation 11: Calculation of Menger curvature using three non collinear points.

where “ $S(z_1, z_2, z_3)$  is the area of the triangle with vertices  $z_1, z_2$  and  $z_3$ . If the points are collinear the curvature is set to a value of 0” (see Pajot, 2002, S. 29)

## 4 General Evaluation Approach of the Catheter Simulation

In the following chapters all steps up to the creation of a complete vessel segmentation module as well as an evaluation module for the comparison of simulated and real catheter path to each other are explained. Additionally, a brief introduction to MeVisLab is necessary to understand the basic functionality of the programming environment that is used to create each module.

### 4.1 MeVisLab as a Platform for Medical Imaging

All the following algorithms implemented in this thesis are developed in MeVisLab. It offers a broad spectrum of developing tools. “Its standardized module principle enables rapid prototyping and offers a wide range of features, supported file formats and extensibility options. The combination of visual programming, Python scripting and C++ programming makes MeVisLab a powerful tool for developers” (MeVis Medical Solutions AG [b]). As can be seen in figure 5 the interface consists of modules, which are mostly equipped with one or even more inputs/-and outputs which can be connected to each other to visualise the data transfer. General purpose modules are reusable, or they can be created specifically for a given task. An algorithm is implemented in each module. Therefore, the connection of modules corresponds to a combination of corresponding algorithms. In the given example an “ImageLoad” module is used to load an image file in order to transport it to the “View2D” module, which visualises the data in a panel. Most modules have panels, as they can be used as user interfaces. In the example in figure 5, the panel of “LoadImage” is used to find the path or filename of the visual information which is then visualised by the panel of the “View2D” module. Combining multiple modules creates a network.

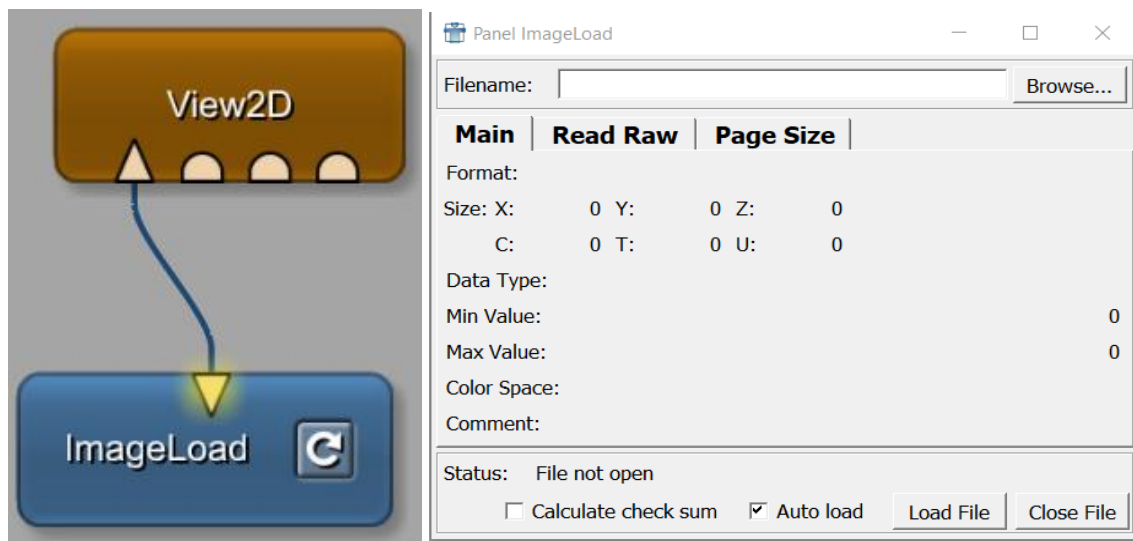


Figure 5: MeVisLab network [left]. Used for loading images with ImageLoad and viewing these images with View2D. ImageLoad panel [right], used to specify the data path that is loaded.

Networks can be encapsulated into macro modules to reduce complexity by binding connected algorithms that are used for a specific purpose together. Not all modules have internal networks, but the ones that have one are similarly structured. They consist of inputs-/and outputs as well as different interconnected modules that change data along the way from the input to the output. Sometimes internal networks are used to reduce complexity, for convenience, or to add multiple functions or modules together, while an algorithm is created in the background to further transform the data streams.

Additionally, programmes connect each internal network with each other. There are two main types of underlying programming inside each macro module with an internal network. The script and the actual algorithm are based on Python or C++. The script is used to define the interface of a module, both for programming and for the user in form of a GUI (Graphical User Interface). It specifies the number of inputs-/and outputs, the type of data each input accepts and the name of each input-/and output. The actual algorithm is defined in another file. It can be written in Python or C++. Only Python is used in this thesis. The algorithm can access data from each input and output of all modules within the internal network. It can change data mid-stream before it accesses the next module. This makes it possible to further manipulate data streams directly. As a part of this thesis several new modules are created.

## 4.2 Methodology of this Thesis

This chapter focuses on the general idea of how to create data to evaluate and optimise the catheter simulation software. In this thesis two different data sets are compared for each different imaging data set. Each data set consists of image data portraying an artificial object that resembles a vessel system, in which a catheter is placed as shown in figure 6. The general approach to prepare the data for comparison is to segment the catheter and vessel system separately. The extracted vessel system is then transformed into its centre line representation, cropped to the region in which the real catheter is located at and changed into a catheter using the previously described vessel path to catheter path simulation algorithm. Both the real and calculated catheter path are then sampled by choosing a sampling distance which then selects a number of data points from the previously segmented catheter path or vessel path respectively. The graphs have a sampling distance based on the image resolution they are segmented from. This set sampling distance is later changed to a sampling distance of 1 mm. Each sampled path consisted of a list of several datapoints with three coordinates, representing x, y- and z-coordinates and additional information concerning the radius of the vessel branch segmented from the vessel graph. After the sampling, both lists are graphically overlapped and cropped to equal initial and end points to further prepare them for comparison. Finally, the distance between the data points in both lists is measured and averaged using a Euclidean distance calculation. The result is an average Euclidean distance value, which is calculated for each data set, respectively. By changing certain parameters which effect the Newton optimisation process, the average Euclidean distance value can be changed. This value is used in the following to visualise an overall change in accuracy within the system, depending on the particular choice of parameters. The lower the average Euclidean distance value becomes, the closer both simulated and real catheter path are to each other and therefore the closer the simulation approach is to reality.

A total of eight sets of imaging data are provided to optimise and evaluate the programme, four from the so-called candle holder phantom and four from three different physiological vessel phantoms, which will be shown in this thesis. Additionally, eight data sets were added to further analyse the possible influence of external forces by using information extracted from camera recordings, referred to in the following as recordings, of an acrylic tube system representing a vessel system.

## 5 Image Data Processing

Chapter five is dedicated to the description of each algorithm that is created to segment the image data in order to acquire a catheter path and a vessel graph for comparison. It gives a deeper insight into the procedure and the fundamentals of data segmentation. The segmentation process is shown here for the candle holder phantom. It is one of four different phantoms that are used as basis for the evaluation in this thesis. The candle holder is chosen because its vessel segmentation contains some additional steps and unique workarounds, in which algorithms especially developed for it are embedded. This is necessary due to the apparent lack of vessel connections as represented in figure 6. Nevertheless, the segmentation of the other phantoms is also described, but in less detail, as many segmentation steps are analogue to the candle holder.

This chapter begins with an introduction to the different vessel phantoms used in this thesis. It then explains the segmentation network used to process the image data sets and segment the vessel graphs and the catheter paths from these images. Furthermore, it describes the overlapping and cropping of excess data points from the real catheter path and the simulated catheter path in order to prepare the data for evaluation. Finally, the recordings used in this thesis to measure the impact of mechanical effects on the simulation accuracy are presented.

Every series of image data used in this thesis is acquired by an Artis Zeego CT (Siemens Healthcare GmbH, Germany). Only the recordings are acquired differently.



## 5.1 Candle Holder

The first set of image data is the so-called candle holder image. It is shown in figure 6. The phantom represents a vessel system and is composed of tubular structures made out of silicon and is fixated with mounts. It is custom made and consists of three vessel paths (two bifurcation). A catheter with a radius of 1 mm is successively moved through each artificial vessel branch. The phantom with the inserted catheter was recorded by the CT for four times. Each time the catheter was in a different vessel branch, which provided four different sets of image data. However, this phantom seems to have connections not visible in the CT between the vessel branches, which need to be added manually later. The candle holder has an image matrix of 512x512 over 394 slices. The resolution is 0,68 mm isotropic.

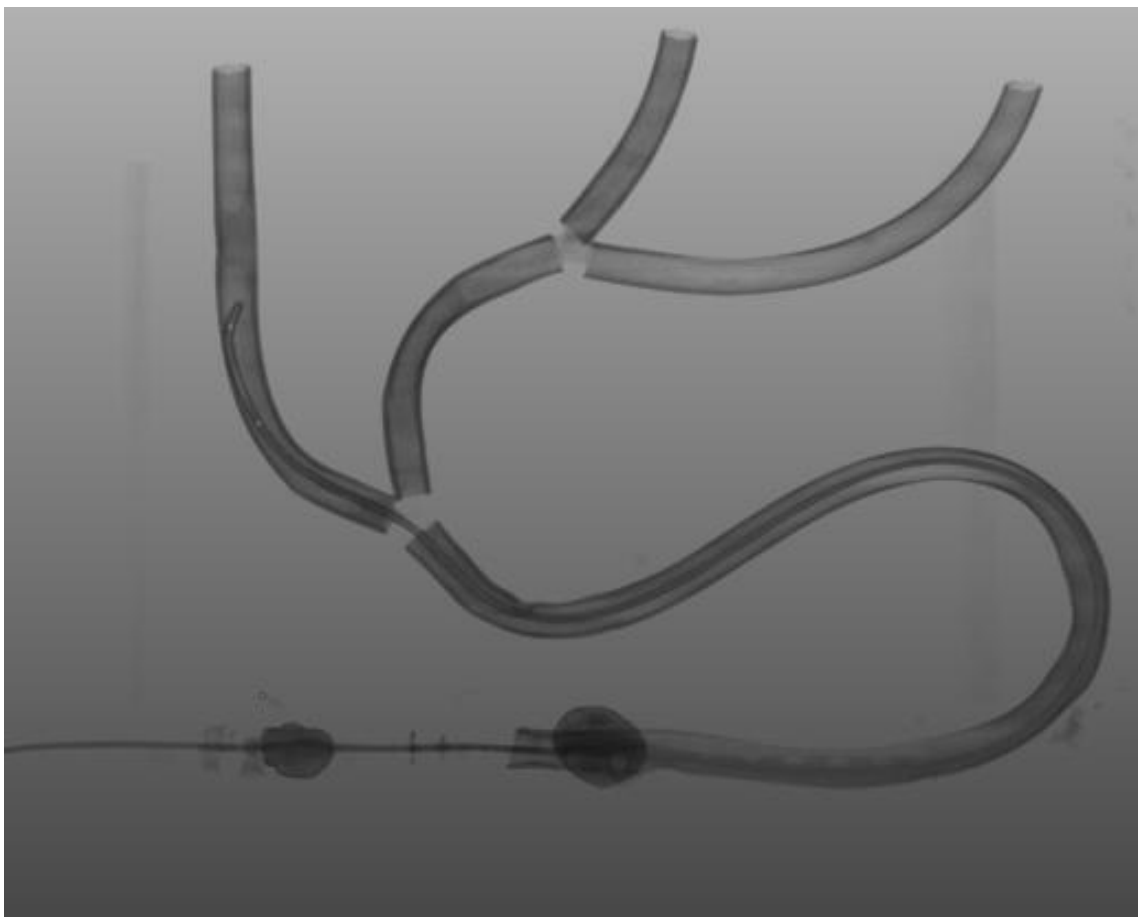


Figure 6: Candle holder vessel phantom used in this thesis for cases 5-8. Consists of a catheter inside of tubular structures made out of silicone, representing a vessel system.

## 5.2 Physiological Vessel Phantoms

In addition, to the candle holder, three vessel phantoms are used in this thesis, as shown in the figures 7-9. They consist of an artificial vessel system with multiple vessel branches, each with varying diameters and curvatures.

One is a physiological vessel representation made out of a rectangular silicone block (provided by the ARCANDIS GmbH, Germany) with a catheter with radius 0,5 mm inserted into it, which is shown in figure 7. It has an image matrix of 512x512 over 393 slices. The resolution is 0,486 mm isotropic. Two image data sets are used from this phantom.

The other one represents the aorta (provided by the United Biologics Inc., U.S.A.) with a comparatively large diameter and a catheter inserted into it with a radius of 1 mm, as shown in figure 8. The last one is another physiological vessel phantom (provided by the United Biologics Inc., U.S.A) as shown in figure 9. A catheter with a radius of 1 mm was inserted into this phantom as well. Both data sets have an image matrix of 512x512 over 394 slices. The resolution is 0,68 mm isotropic.

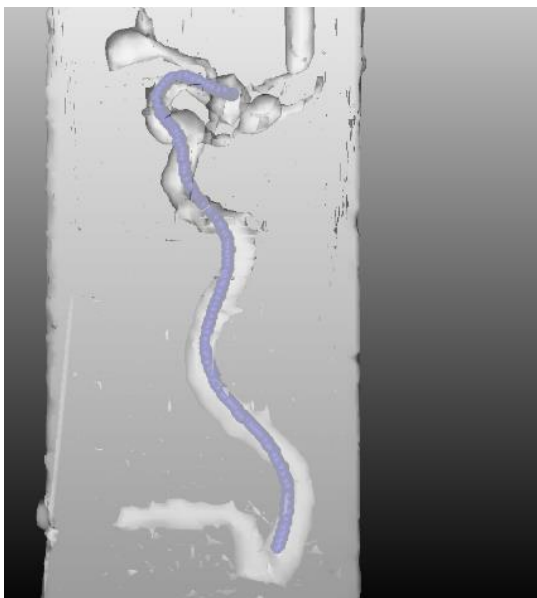


Figure 7: Physiological vessel systems: Phantom 1; cases 1-2. Provided by the ARCANDIS GmbH, Germany.

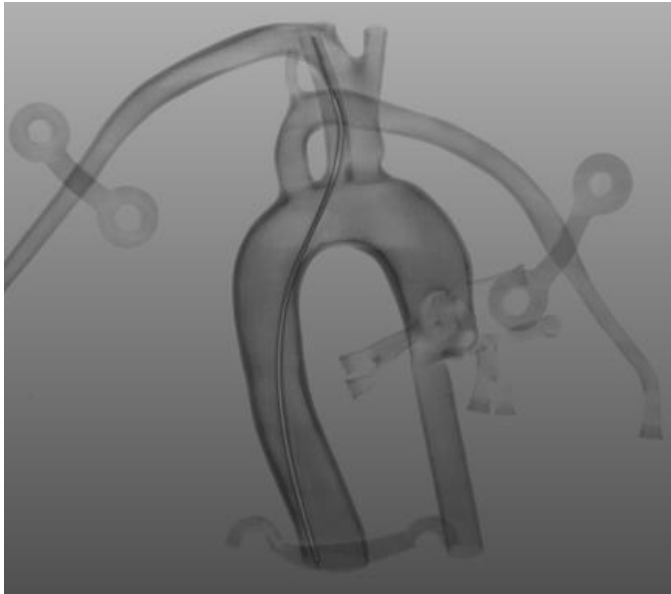


Figure 8: Physiological vessel systems: Phantom 2; case 3. Provided by the United Biologics Inc., U.S.A.

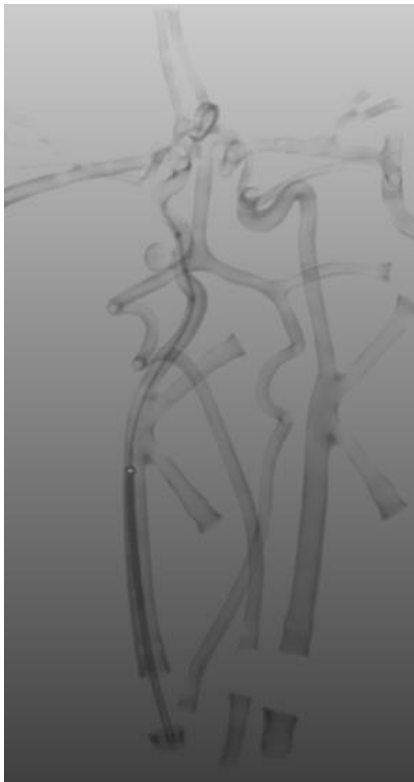


Figure 9: Physiological vessel systems: Phantom 3; case 4. Provided by the United Biologics Inc., U.S.A.

### 5.3 Camera Recordings

The last image data provided for this thesis is a vessel representation made of bent acrylic glass, which is shaped to represent a vessel system with five different vessel branches which have an area of 400x400 mm, as shown in the figure 10. A catheter is guided through each vessel branch, while a FLIR BLACKFLY S BFS-U3-31S4 camera is placed 500 mm above the centre of the phantom to record the insertion of the catheter and the navigation process. The distance is specifically chosen to maintain a 1:1 ratio in terms of distance measurement inside the phantom. Here, 5 voxels correspond to 1 mm, respectively. The results are eight different recordings of catheter movement through a vessel representation. One frame is illustrated in the figure 10.



Figure 10: Camera recordings of a catheter moving inside an acrylic tubular structure. Used in this thesis for analysis of mechanical influences.

The volumetric image of the phantom is acquired with a Siemens Magnetom Skyra 3T (Siemens Healthcare GmbH, Germany) using a gradient echo pulse sequence (mprage) and an image matrix of 384x384 over 48 slices. The voxel size in the acquisition is 1 mm isotropic. The vessel system on this image is segmented manually prior to this

thesis. Using the segmented vessel system in combination with the extracted catheter movement from the recordings enables catheter simulation evaluation. These recordings are used to show possible differences in the accuracy of the catheter simulation between pushing and pulling a catheter. The vessel representation is custom made and consists of five vessel paths (four bifurcation).

## 5.4 Imaging Data Segmentation (Candle Holder)

For the evaluation of the catheter simulation a segmented catheter and a segmented vessel path is needed to apply the vessel path to catheter path simulation to. A MeVisLab network is created to extract the images of both structures from the given set of imaging data files, available in DICOM format. The network can be divided into six groups or subsections. Each group serves a specific purpose and is represented by a chapter in this thesis. At first the separately stored image data files are loaded into the system, where each image slice of each case is stacked together to create a three-dimensional spatial representation of the image. Outgoing from that are two different paths the imaging data is guided to and processed.

### 5.4.1 Catheter Segmentation

The first subsection described in this thesis is dedicated to the catheter segmentation. This subsection is responsible for segmenting the real catheter from the image and then sample it to use it as a reference for the evaluation and optimisation process.

The principle is to prepare the loaded data set for the region growing process. Region growing, as described in chapter 3, subsection 3.1.2, is a process in which a seed pixel is selected in an image which grows indefinitely until the stopping requirements are met. However, before region growing can be successfully used on an image, the image must be prepared as described in the following:

1. A threshold is used to eliminate grey values not associated with the catheter. In this case, the catheter usually has higher grey values, than the surrounding artificial vessel material. Thus, by adjusting the lower threshold to a sufficiently high value, big parts of grey values not associated with the catheter are cut out.

However, there are still a few points which, although not related to the catheter, still fall inside the range that is set by the threshold. To cut out all excess data points, the steps 2, 3, 4 and 5 are added.

2. A Sobel edge detector is used to perform a gradient magnitude estimation of the previously filtered image. It is used to determine the gradient magnitude of each data point by using the “sum of the kernel or matrix convolutions, that are written into the output image, which is a grey value image representing the strength of the gradients in each voxel” (see MeVis Medical Solutions AG [d]). In this case the use of a Sobel edge detection operator makes it possible to distinguish and thus to filter parts that are not associated with the actual catheter. The application of this method improves the separability of different areas within the image. Which leads to a much better region growing result as seen in figure 11-12, due to the clear separation by image borders associated with other volumes.

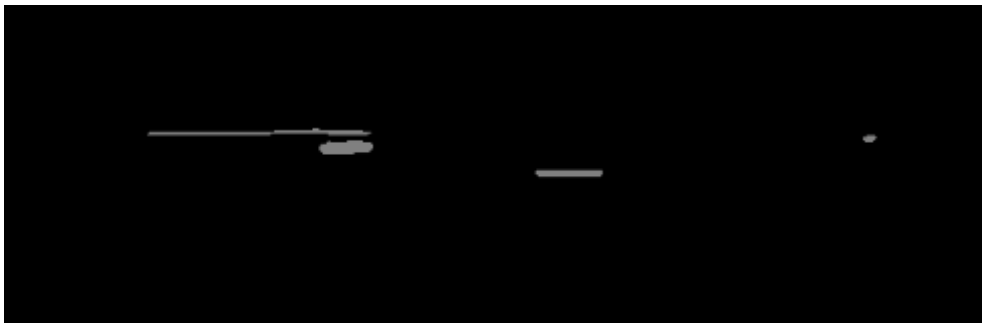


Figure 11: Image data for catheter segmentation after threshold was applied and before applying Sobel to get clearer boarder separation.

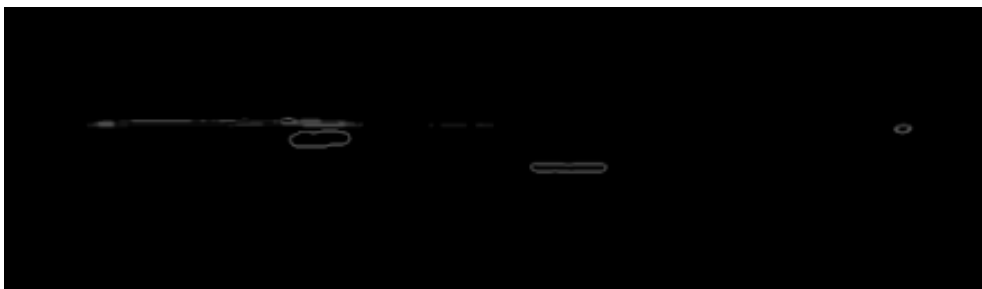


Figure 12: Image data after applying Sobel for better separability between catheter and access data points.

3. Excess image data was eliminated by adjusting the dimensions of the three-dimensional box in which all information for this image is stored, hereafter referred to as the bounding box. This is primarily used crop out the lower end of the candle holder image, as shown in figure 6, as these candle holder images

have several fixations to mount the artificial vessel system. These fixations are located at the lower end of the image. They can be excluded by changing the size of the bounding box in y- direction. In addition, by further adjusting the image in all dimensions, the computational strain on the program can be reduced, as there is less space that carries no valid information for the segmentation, to calculate through.

4. Another threshold is used again, but this time not with an interval but with a minimum value of 0.2, as the gradient magnitude values created from Sobel range from 0 to 1. By using a new threshold again, outliers that seem to have values less or equal to this threshold are cut out to improve the segmentation. The use of a threshold is necessary and successful for this. There are some regions on the final catheter showing holes, since not all pixel with a grey value less than 0.2 are located outside the catheter. This results in a segmented catheter with holes in it, possibly disrupting the segmentation and therefore the evaluation at one point.
5. To prevent holes in the phantom caused by the previous thresholding, a method called closing is used. Closing, as described in chapter 3, subsection 3.3, is a morphological process in which a dilation and erosion are used successively in image processing. Closing is capable of filling holes in an image without widening the image border itself.
6. A region growing operation is applied, which is able to find connected parts inside an image. By manually selectin a starting position (seed) and selecting the “neighbourhood”, the module locates the surrounding data points connected to the starting positions in that slice and then finds data points connected to the starting area throughout all image slices consecutively as described in chapter 3, subsection 3.1.2. Finally, it generates an image that shows only the connected data points that are calculated. All additional data points not associated to the seed pixel, are filtered out of the final image.

With these different methods it is possible to segment an exact representation of the real catheter from the candle holder as shown in figure 13.

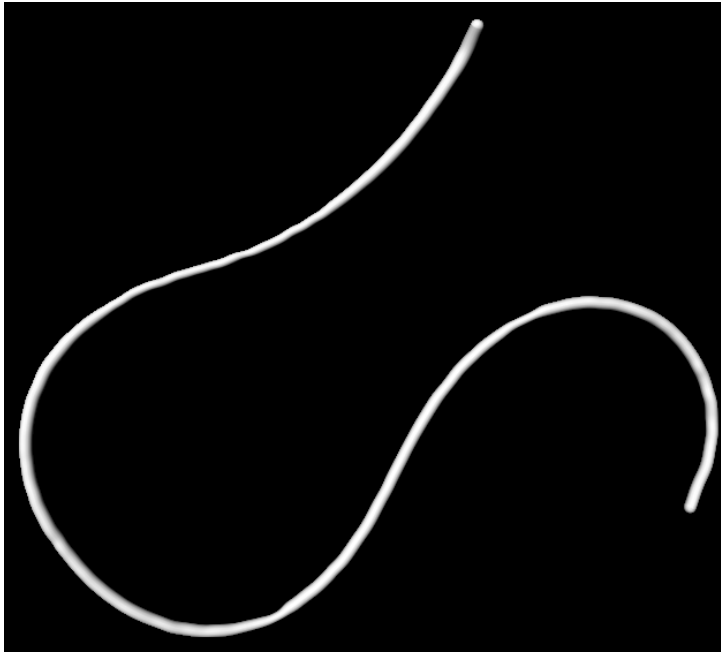


Figure 13: Segmented catheter mask representing the catheter located in the image data, respectively. Later sampled and used as the real catheter path for the evaluation process.

#### 5.4.2 Catheter Skeletonization and Sampling

As explained in the previous chapter, the output of the catheter segmentation consists of a series of image files, that have been manipulated to show only the catheter inside. However, the data type still has to be changed. In order to compare it to a calculated catheter. Mainly, sampling is required to splice the figure into numerous data points, each with x, y and z coordinates. The previously created catheter segmentation data must be skeletonized and sampled to be prepared for the comparison with the simulated catheter path. The first step is to compute the “skeletonization of a binary image by successive erosion of border voxels” (MeVis Medical Solutions AG [c]). It is important to mention that the “topology of the initial mask is preserved” (MeVis Medical Solutions AG [c]). The skeletonization is necessary to ensure reasonable sampling by smoothing the border voxels of the image. After skeletonizing the catheter image, it is sampled. The sampling distance is adjusted to a value of 1 mm. It was concluded that lowering the sampling distance even further has only a marginal effect on the evaluation result (ranging in the lower hundredths of a millimetres), while the computational strain on the algorithm automatically increases.



In addition to the sampling, the trailing edges, which occur in the course of skeletonization, are cut. These trailing edges consist of multiple little branches at the end of skeletonized image. These edges are excluded by intention as they can potentially falsify the error calculation. After removing the trailing edges and sampling the catheter path, the image looks as shown in figure 14. In MeVisLab this final image is now called an XMarkerList. As the name indicates, these lists consist of markers which all have spatial position values (x, y, and z) and values concerning the radius of the sampled graph. The radii from the segmented vessel graphs are used for the catheter simulation process and are crucial for the optimisation and evaluation of the simulation.

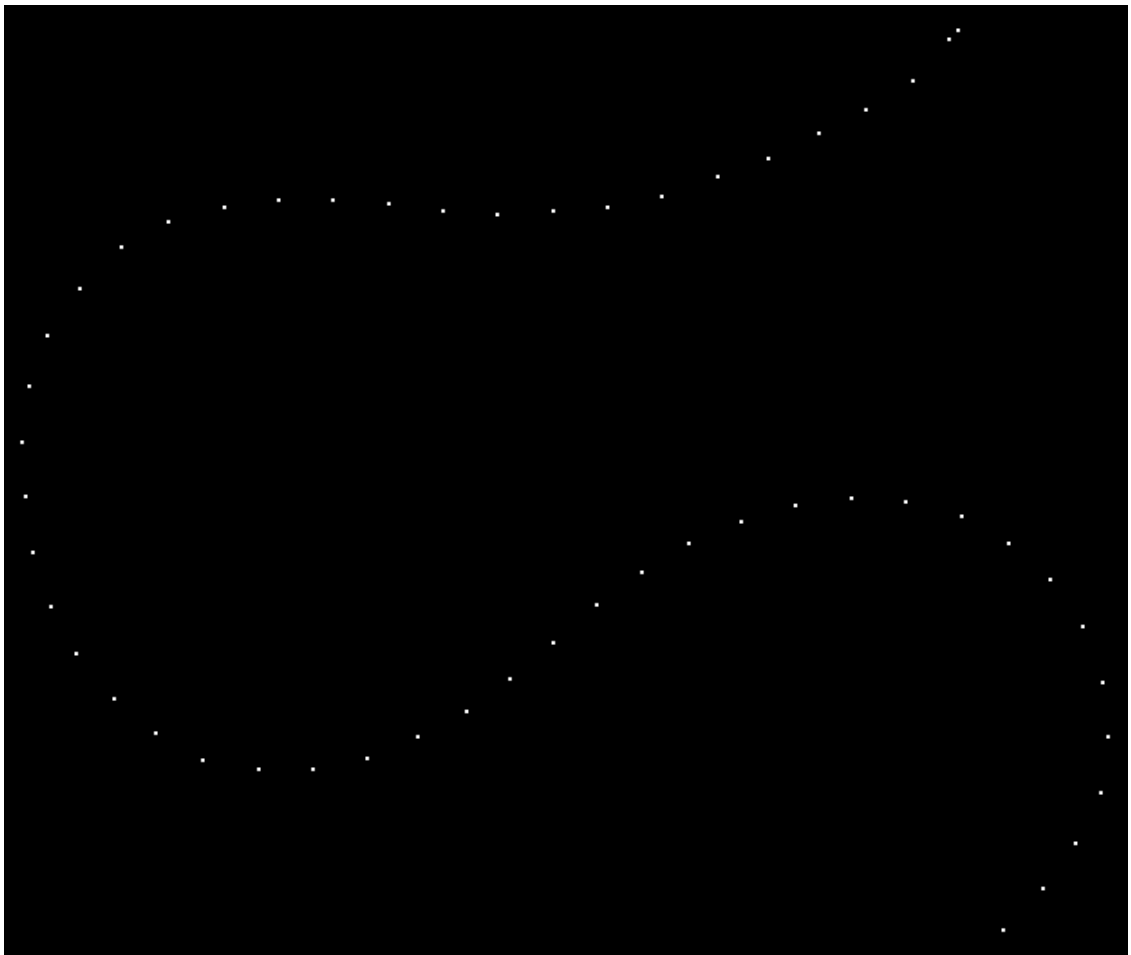


Figure 14: Segmented catheter path after sampling. Each point represents one marker position in the generated XMarkerList.

### 5.4.3 Inner Vessel Segmentation

The other path the loaded imaging data files take leads to vessel segmentation. In this path, the aim is to segment the vessel system of the imaging data, to then transform it into a centre line representation, and afterwards transform them into a simulated catheter path for comparison with the real segmented catheter path. As mentioned before, the inner vessel segmentation for the candle holder phantom is described in the following. Due to the invisible connections between vessel branches of this phantom a specific segmentation procedure is developed in order to add the missing connections to the overall vessel system.

The idea is to add in seemingly missing three-dimensional structures occurring at the vessel connection points of the candle holder. The “CreateObject” module is created in order to solve this issue. The network first loads the image and visualises it, at three different angles called coronal, sagittal and axial as shown in figure 15. This representation is then used to manually implement markers within the image. These markers are then used as a reference to calculate tubular structures with a grey value of 1 and a set radius chosen beforehand that follows the set path provided by the markers. It is important to have the original vessel system as a reference to ensure that the generated volume is in the right location inside the vessel system.

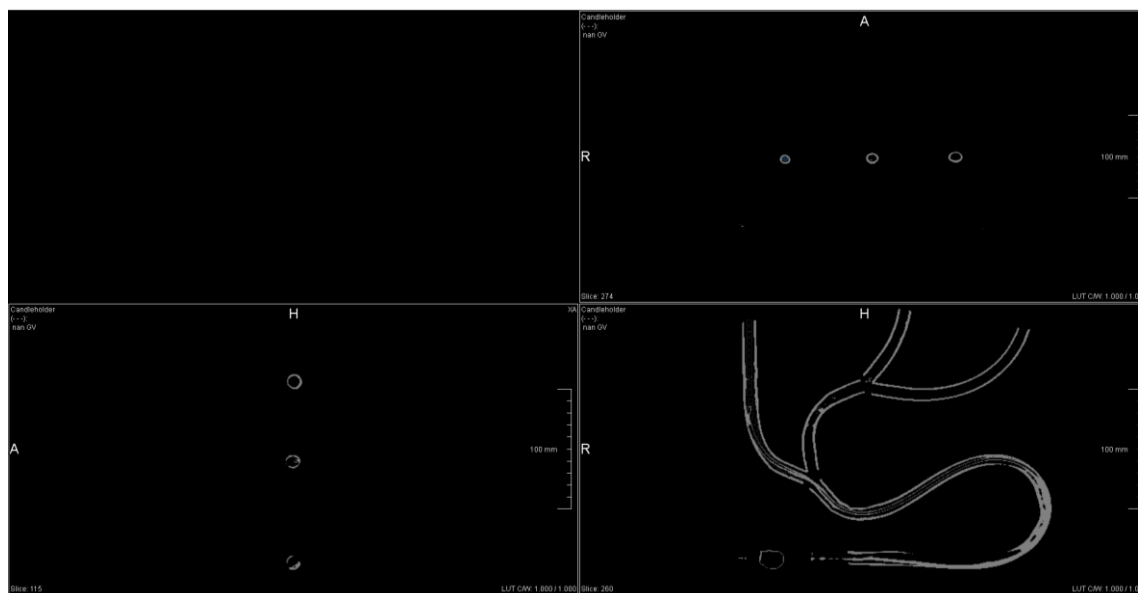


Figure 15: CreateObject interface for generating three-dimensional structures inside the vessel.

After explaining how the “CreateObject” module works, the overall method of segmenting the inner vessel volume of the candle holder can be explained in its entirety. The

functionality is divided into five steps. The result of these five steps is a complete extracted inner vessel system from the candle holder. Similar to the catheter segmentation, the main goal is to prepare the image for the region growing process, by extracting only the relevant image information. In this case, the inner tubular vessel system.

Prior to the vessel segmentation process, a threshold followed by a dilation and a closing operation is used to filter out data not associated to the vessel system of the candle holder phantom. The image after dilation is used as reference for the created object module. The output image of the closing operation is used to be subtracted from the artificial tubular structures from create object. Due to the thresholding the original image is now a binary image

Step one:

For each vessel branch, a corresponding "CreateObject" module is used to implement tubular structures within the hollow tubular vessel system. These structures, given an appropriately set radius should then represent the inner volume of the vessel. The objects created in this way need to have a slightly bigger diameter and the same curvature as the volume of the inner vessel to ensure better segmentation, which will be mentioned later.

Step two:

After creating these tubular structures they are subtracted from the real vessel structures of the image. This is done by simply subtracting each grey value from the corresponding grey value of the other one. In this case, the real and generated vessel structures are overlapping. Thus, subtracting both from each other results in an accurate representation of the inner vessel system.

Step three:

An additional interval threshold is set to further segment the created image. Here, the subtraction of both images in general leads to negative values as soon as the subtracted grey value is larger than the other. To get rid of the negative values, the threshold is set to have a lower interval value of 1, which cuts out any negatives.

Step four:

Region growing is used to further segment the created inner vessel structure. Region growing, as explained in chapter 3, subsection 3.1.2, is capable of segmenting a volume of connected pixels. Here, the chosen volume, is the segmented inner vessel structure. The selection of the inner volume of the vessel, resulted in the region growing module that ignores any outlying grey values. Thereby an accurate inner vessel representation is delivered.

Step five:

Step five consists solely of adding all created inner vessel structures. They can be used as the basis for the next step, which is the creation and addition of the missing structures, that connect the vessel phantom.

#### 5.4.4 Adding missing Vessel Connections

After extracting the inner vessel structures, the missing connections between vessel branches need to be added, to ensure that a complete vessel system is obtained. To achieve this, the “CreateObject” module is used once again. In this case, it is not used to create a tubular structure inside the vessel, but rather to connect different vessel branches with each other in three-dimensional space. The radius in this case has to be manually adjusted and is set to be equal to the already created inner vessel system. In the end, all created branch connections as well as the previously created inner vessel representation are combined by adding them together, to form a complete vessel system representation. This constitutes the basis for the simulation of the catheter path.

#### 5.4.5 Graph Manipulation

The next step after the creation of the inner vessel system and successful addition of the branch connections, is to further prepare the vessel system manually, to ensure an accurate vessel path for the catheter path simulation. The skeletonized graph, as shown in figure 16, is not consistently smooth and shows lot of additional data points, which might possibly disrupt the underlying newton optimisation process for the catheter path creation.

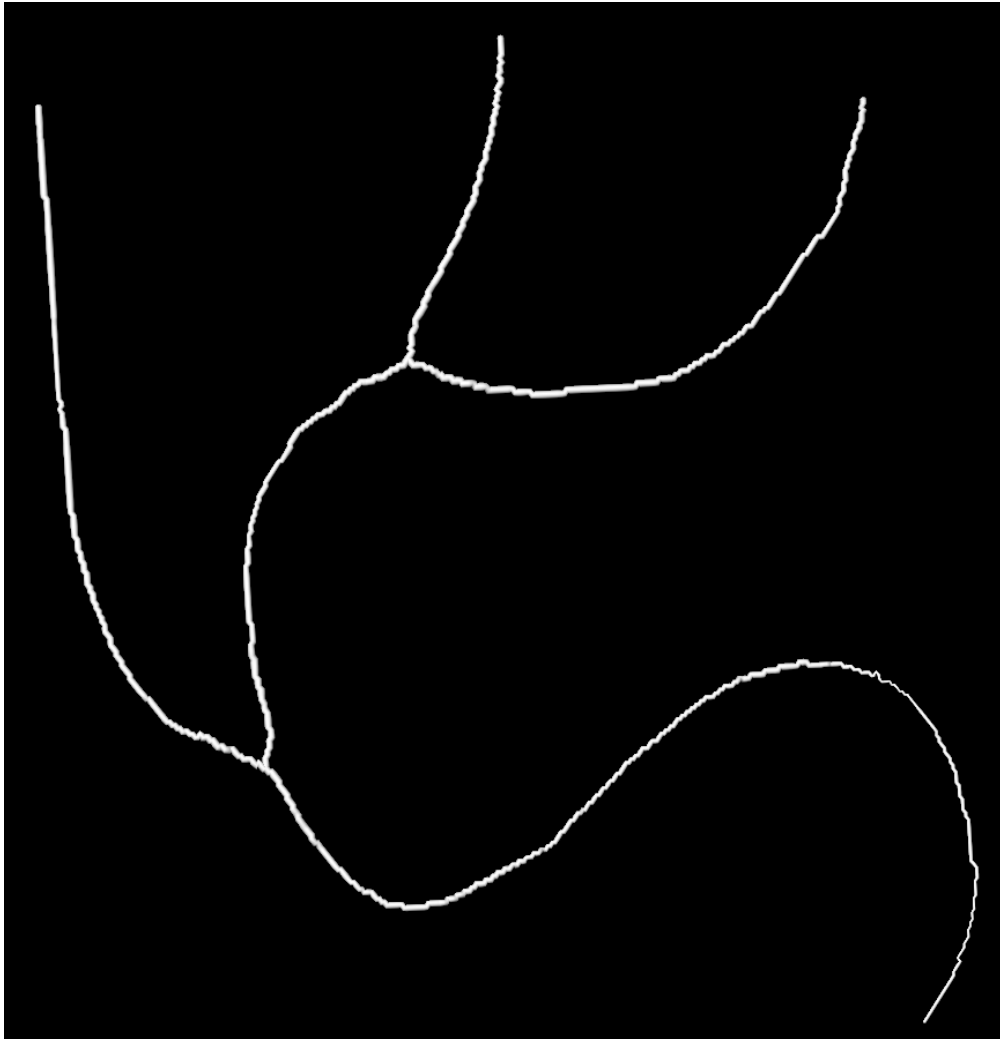


Figure 16: Skeletonized vessel graph representation of the candle holder image. The skeletonized vessel graph representation is not smooth and shows additional data points that need to be excluded for accurate vessel graph to catheter path simulation.

It is therefore necessary to further change the image. The image processing is performed by a graph manipulation tool provided in MeVisLab. With this tool, it is possible to access certain areas inside the skeletonized vessel graph and remove them as well as smooth the entire graph. This is beneficial for the later catheter path simulation. The final vessel centre line representation of the entire vessel system is shown in figure 17. Although it occurs like a system with a constant vessel diameter, additional information is hidden inside each vessel graph. It carries not only spatial information's, it also contains data about the radius of each point in it, representing the vessel diameter at each position. This is of high value, because the vessel diameter is used as a bounding condition for the catheter path simulation. This simulation uses the diameter value stored in each data point as an instrument to decide how much the simulated catheter path can be altered in its shape during its creation. Limiting the radius in which the simulation can operate

ensures that the calculated curvature minimising catheter path is still located inside the vessel system.



Figure 17: Candle holder centre line of the segmented vessel graph.

Additionally, only one vessel path is selected, as shown in figure 18, to fit the given catheter path. The other vessel branches are deleted.

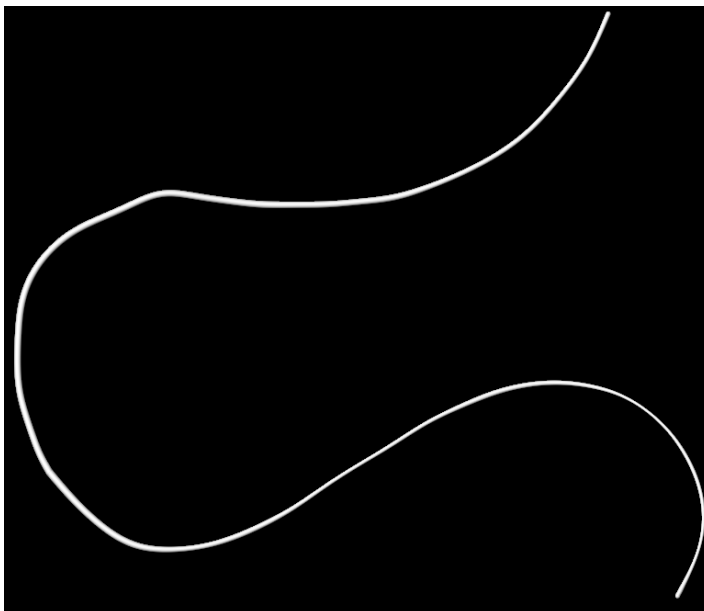


Figure 18: Candle holder vessel graph after graph manipulation. Only vessel branch in which the catheter is located is left.

#### 5.4.6 Graph Root detection and Sampling

After segmenting the inner vessel system, connecting the branches manually, smoothing the vessel graphs and selecting the correct vessel branch, the last step is to edit the graph root. The graph root is implemented in the created vessel graph and tells the catheter simulation algorithm where the base of the graph is located. Based on this information, the catheter path simulation is performed. To ensure that the simulation starts at the right position and therefore uses the complete vessel graph and not just parts of it, the graph root is selected explicitly. This is done by loading the original image and manually setting a marker at the beginning of the catheter to represent the root. From this marker, spatial information's are transferred to the extracted vessel graph, which then uses this spatial information to set a new root. Since the vessel graph is extracted from the original image, the spatial informational distribution stays consistent and therefore is interchangeable. The resulting vessel graph finally is sampled. By default, the output of the skeletonization is a vessel graph that is sampled according to the image resolution. Applying another sampling distance enabled the vessel graph to be down sampled. This is done in this thesis to change the sampling distance to a value of 1 mm for each vessel graph segmented. This value results in an accurate graph representation judging with respect to the visual output of each catheter path used in this study. A further decrease of the sampling distance leads to a disruption of the Newton optimiser embedded into the catheter simulation algorithm. This in consequence resultes in a loss of information. This issue will be discussed in chapter 6, subsection 6.1. After sampling the vessel graph is called a vessel path.

#### 5.4.7 Other Phantoms

As mentioned at the beginning of chapter 5, subsection 5.1-5.3, there are three other vessel phantoms that are used for this thesis and one vessel representation made of acrylic tubes, previously described as recordings. The three phantoms represent a more physiological vessel system, and the other one is a series of recordings of a catheter moving through a vessel representation, consisting of a system of acrylic tubes, as mentioned in chapter 5, subsection 5.3. The segmentation of the more realistic vessel phantoms shown in figure 7-9, follows the same procedure for catheter segmentation as the candle holder phantom. The only exception is Sobel and the second threshold. Not

every physiological vessel system needs a better border separation provided by Sobel or a second threshold after Sobel to eliminate unwanted pixels. It depends on the visual data output and the grey values the catheter has. However, the segmentation of these vessel system is different. Two different approaches are needed. One for the aorta representation, figure 8, because of its immense inner vessel diameter and the narrow, convoluted vessel structure of the phantom shown in figure 9. One for the remaining physiological vessel phantom in figure 7, excluding the recordings. The vessel system in figure 7, is segmented by firstly extracting the catheter inside the vessel using a threshold. The remaining vessel system is then overlapped with a big tubular object, filling the entire image, created by "CreateObject". By subtracting the grey values of two images from each other, where one image is the previously created object and the other is the remaining vessel structure, produced a visually accurate segmentation of the inner vessel system combined with many excess grey value areas outside the vessel. Removing most excess data points was done by adjusting the bounding box dimensions. The reuse of region growing removed the remaining unwanted grey value areas outside the vessel by selecting a pixel in the catheter as the seed. Finally, the holes in the inner vessel structure, due to previous thresholding are filled with a closing operation. The steps described in chapter 5, subsection 5.4.5-5.4.6 are analogue for these type of images

The segmentation of the remaining two vessel phantoms requires an alternate approach. The inner vessel contour of the image needs to be manually drawn throughout each slice to keep the varying diameter and convoluted vessel graph information. Using the same method as mentioned before proved to be insufficient and was not capable of reliably extracting the inner vessel structure due to its unique form. The drawn inner vessel representations are therefore manually arranged inside the phantom and stacked on top of each other, as shown in the figures 19-20.



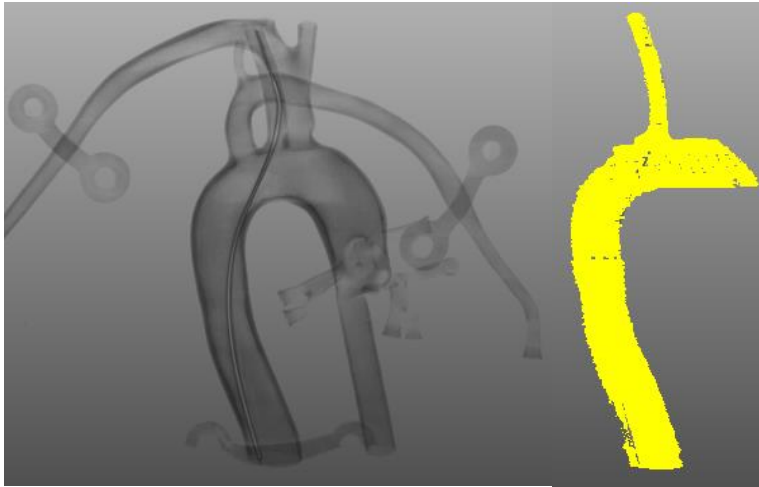


Figure 19: Aorta vessel phantom (left) and, extracted inner Vessel Structure (right). Used for vessel segmentation.

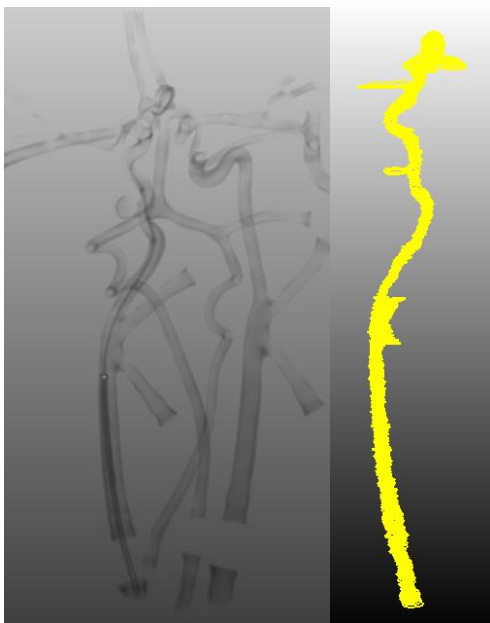


Figure 20: Physiological vessel phantom (left) and extracted inner vessel structure (right). Used for vessel segmentation.

This set of stacked vessel contours represents the inner volume of the vessel and is transformed into a three-dimensional object. This object is then skeletonized and used as a vessel graph. The following steps are analogue to the steps described in chapter 5, subsections 5.4.5-5.4.6.

The recordings are different. The vessel graph is already given and just needs to be skeletonized and further manipulated in terms of smoothness, path selection and sampling distance as in chapter 5, subsection 5.4.5-5.4.6. A network is provided which is capable of detecting the catheter inside each recorded frame and then approximate it by using multiple data points along its path. By using this network, it is possible to

segment the catheter at any given frame in the recordings, therefore changes over time can be analysed. This results in an analysis of the changes in the catheter's curvature with regards to pushing and pulling forces.

#### 5.4.8 Final Data Structure

In summary, the resulting images extracted from an image data set are:

A segmented and sampled catheter path and a centre line representation of the vessel path. The usage of these two images for each visual data set, enables a precise evaluation process and optimisation of the simulation module. In figure 21 the final segmented and sampled real catheter path is shown. It is represented in red colour and the corresponding catheter path simulated by using the vessel path as basis is visualised in blue.

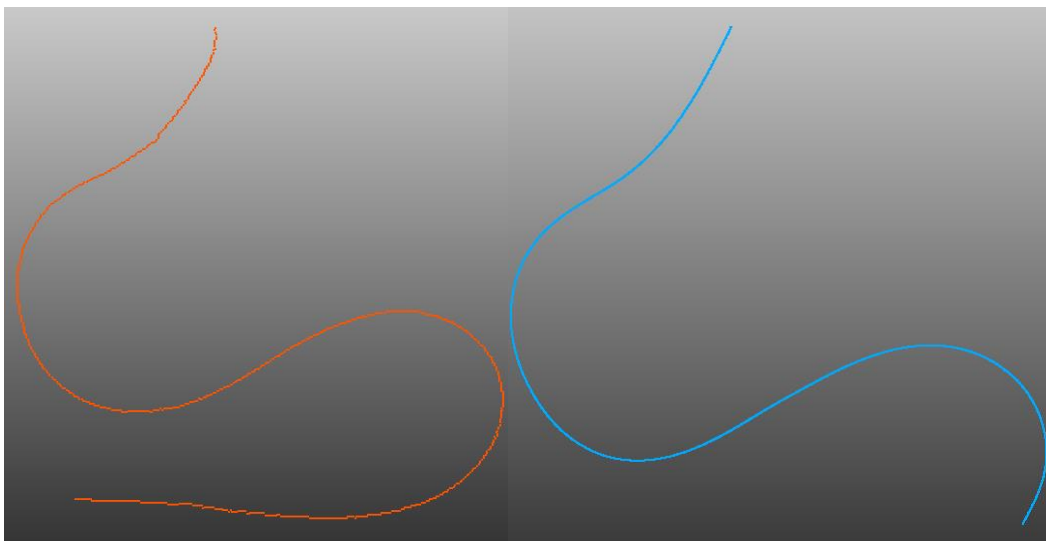


Figure 21: Sampled catheter paths, real (left), simulated (right).

## 5.5 Overlapping and Cropping Catheter Paths for Evaluation

After segmenting the real catheter path and generating the simulated catheter path for each case, the comparison of the two still cannot be made without further modification. Both paths need to be trimmed to an overlapping area to ensure reasonable comparison. As represented in figure 22, simply inserting both XMarkerLists of the simulated catheter path and the segmented catheter path into a common coordinate system would lead to an exaggeration of the error values.

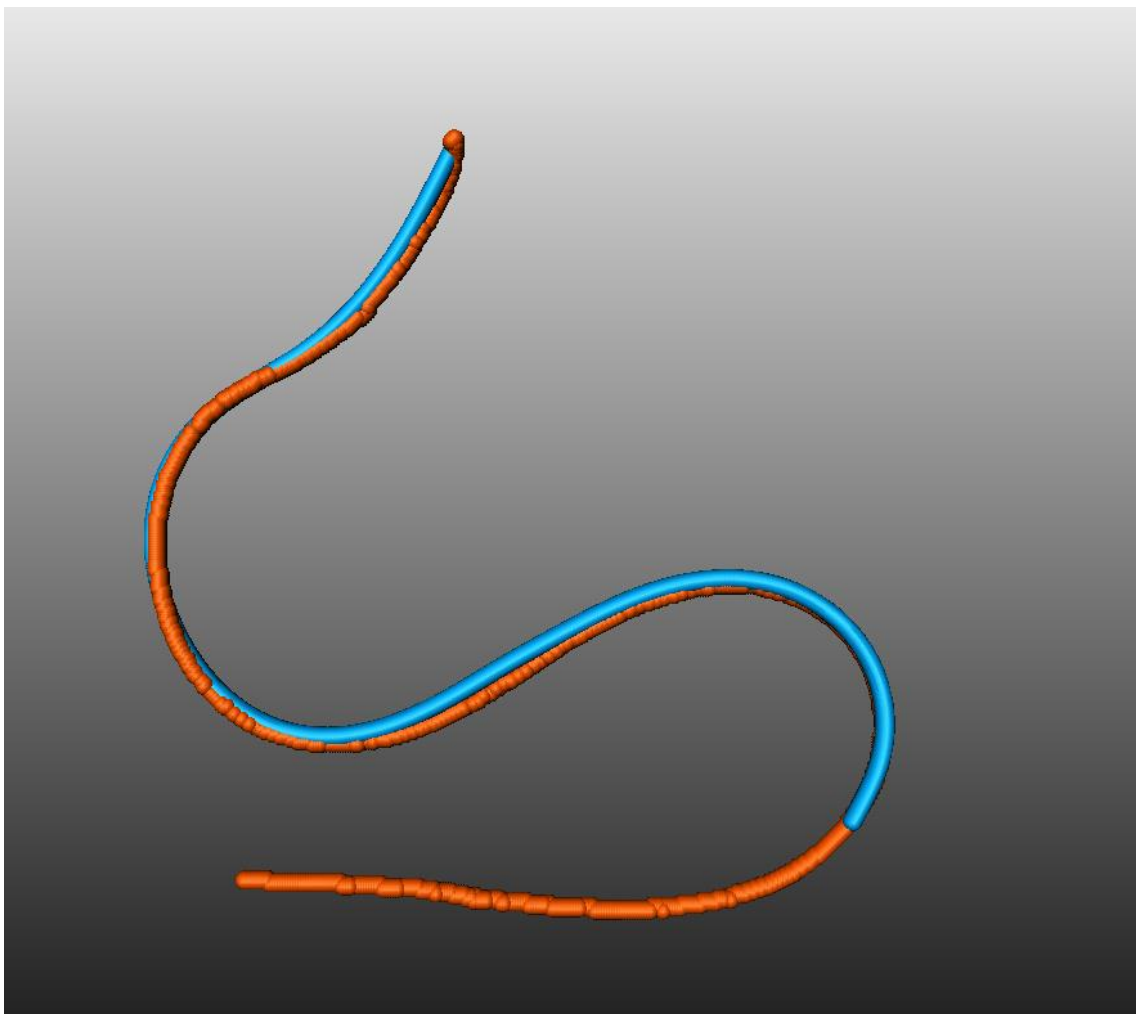


Figure 22: Overlapped catheter paths. Visualizing different starting positions for each catheter path. As a result, start and end positions are cropped to align.

A comparison of these catheter paths without adjusting them to each other's length, leads to a Euclidean distance error composition where the average error is exaggerated by the excess data points. A complete MeVisLab network is created for the sole purpose

of finding excess data points and cutting them out. Using this network, the error can be drastically reduced.

The idea behind overlapping and trimming two XMarkerLists is to make use of the bounding boxes of each sampled image. Each image that is used in this thesis “lives” inside a bounding box. This box describes the volume or area in which all information is stored. Mostly all data sets had three-dimensional bounding boxes, with exception of the recordings, which had two-dimensional bounding boxes. Each image has its own bounding box. Although the extracted catheter paths and the vessel paths, are from the same set of image data, they do not have the same bounding box sizes due to the difference in shape. Having different sized catheter lengths therefore changes the bounding box sizes.

As a result of their extraction from one set of image data, their bounding boxes overlap. Using the intersection area of both boxes is the key to successfully locate and trim the excess data points, which are located outside the intersection area. The lower left and upper right corners of each bounding box are compared to an overall world coordinate system provided by the original image data. The origin of the world coordinate system is used to determine the intersection area. Using vector lengths from the world coordinate origin to the lower left and upper right corner of each bounding box respectively makes finding the intersection area of both boxes possible. The lower left corner of the intersection area is the furthest to the world coordinate origin and for the upper right corner it is reversed, here the right corner closer to the world coordinate origin is the right one. The now calculated corner coordinates of the intersection area are then used to create a rectangular volume that filters out data points outside the calculated corner coordinates for each catheter path. Sometimes only one path was trimmed and sometimes both were trimmed. Sometimes, cutting out the intersection area, results in removing markers at the edge of the intersection area that should not be removed. Hence, a margin value is implemented and adjusted. This margin value includes markers into the intersection area despite their location outside by increasing the size of the bounding box of each catheter path separately. Changing the corresponding bounding box resulted in increasing the intersection area and therefore including the cut values.

At first the bounding box approach was applied to all imaging data analysed in this thesis, as well as the acrylic tube vessel representation used in the recordings. This proved to be insufficient. The issue lays in the attempt to automatise the bounding box cropping in combination with the margin adjustment process. The ideal margin for each setting is

chosen by analysing the average Euclidean distance value between the resulting original catheter path and the simulated catheter path. The idea was that the lower the average Euclidean distance value is, the better the comparison will be and therefore the better the margin. Ranging a margin value from 1 mm to 5 mm for both bounding boxes and calculating the average Euclidean distance value for every margin combination results in a list of values with corresponding margin settings. The margin setting for the lowest average Euclidean distance value of this list was then used as ideal. This is where the issue lies. This approach works well if the compared catheter paths are comparatively close to each other, as in the recordings due to the narrow, mostly straight, and closed vessel representation. Removing relevant values by setting a wrong margin value results in worsen the average Euclidean distance value in that case. However, this is not the case for the other image data. Here the vessel system often has varying diameters (case 3), a complex three-dimensional convoluted curvature structure (cases 1, 2 and 4) or missing connection (cases 5-8). These properties can easily interfere with the approach of automatic margin adjustment, as the calculated catheter paths vary greatly in shape compared to the real catheter path at the beginning. Therefore, a different approach is chosen.

To be sure that the margin adjustment for each set of recordings is accurate, the output is visually examined throughout all data sets.

For the physiological vessel phantoms and the candle holder, the catheter paths are trimmed manually. By visualizing them inside the same panel, as shown in figure 22 and cutting out any additional data points capable of disrupting the Euclidean distance calculation manually. This ensured that the catheter paths are all sufficiently cut and prepared for later comparison

Using these methods made it possible to crop excess data points from both catheter paths, making a reasonable evaluation possible.

## 6 Evaluation and Optimisation of the Simulation Approach

After preparing all given image data sets, the catheter simulation can be evaluated. This chapter will give a deeper understanding of the underlying evaluation and optimisation approach as well as the parameters embedded into it that are used and tuned in this thesis. Additionally, the parameters outside of the simulation that are analysed as well are presented.

### 6.1 Simulation Algorithm and Simulation Parameters

The creation of a given vessel path to a catheter path, that resembles its real counterpart was repeatedly mentioned in this thesis. The underlying mathematical principle of a Newton optimiser was explained as well in chapter 3, subsection 3.6-3.6.2. Following, the parameters embedded into the optimisation process as well as the parameters analysed in this thesis outside the optimisation process will be presented.

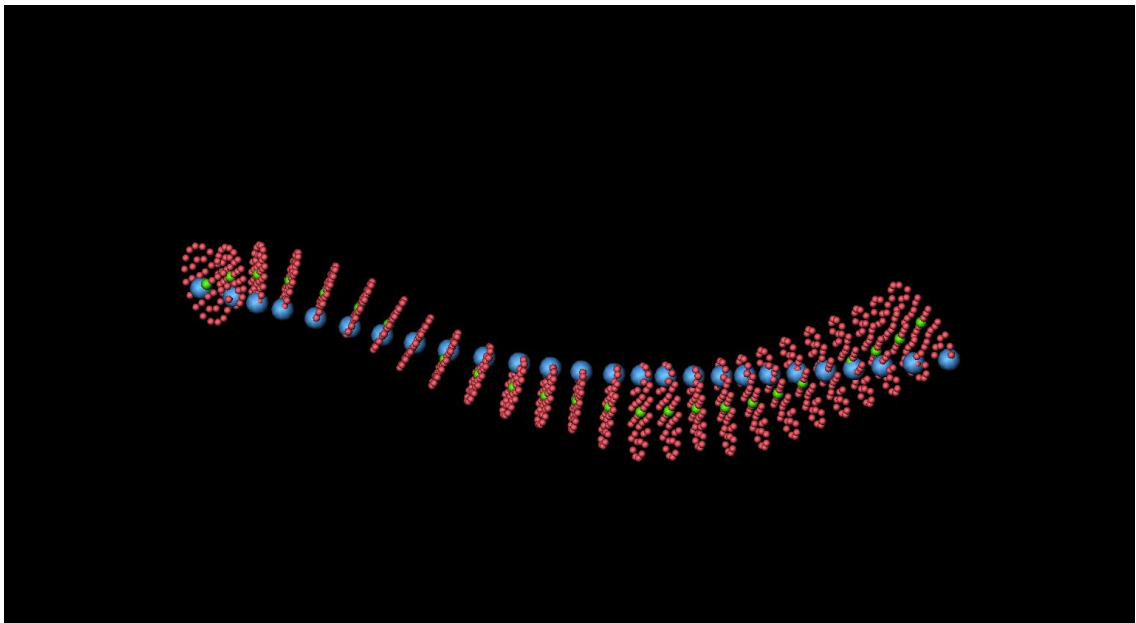


Figure 23: Vessel graph to catheter path simulation. The red dots represent the inner vessel diameter and the green dots the centre line of the segmented vessel. The blue dots are the simulated catheter path.

Figure 23 visualises the principle of Newton optimisation used in this thesis for curvature minimisation, applied to a catheter path. The green dots represent a sampled vessel path centre line which is used as starting value. The blue dots represent the final calculated catheter path after the optimisation process and the red dots around each vessel paths

data point represent the inner vessel structure, provided by the vessel radius from the vessel system segmentation. These inner vessel representation data points (red dots) are important information the Newton optimiser can utilize to minimise the overall curvature of a simulated catheter path, as they represent the points to which each marker position can be shifted. Every newly created catheter path which is generated by the simulation can only consist of the data positions given by the red dots in figure 23. The principle of the Newton optimisation method to generate a curvature minimising catheter path was explained in chapter 3, subsection 3.6-3.6.2.

At this point it is important to mention that the curvature summation process is influenced by the sampling of the vessel graph. Choosing a small sampling distance could lead to the red dots, shown in figure 23, overlapping when high curvature occurs. If this happens, the optimiser evaluates angles between data points, which positions are reversed due to the overlapping, which leads to falsifying the result. The optimiser is programmed to exclude data points that overlap from the catheter path creation process, resulting in high sampling distances in these areas. Therefore, the sampling distance in the case of the vessel path, which the optimiser uses as basis for the vessel path to catheter path simulation, is chosen to be 1 mm. It shows a reliable catheter path output that has no dropped points along its path and that resulted in a simulated catheter path with no missing points. Because, the vessel path should not have a small sampling distance, the created catheter path has to be interpolated afterwards to ensure a correct calculation of the Euclidean distance, which is analysed in chapter 6 subsection 6.3.

The optimisation approach can additionally be influenced by the number of maximum evaluations that are performed, as well as limiting the amount of maximum optimiser iterations and minimum improvement.

The basis for the simulation of a curvature minimising catheter path are three parameters. These parameters are strategically modified in order to analyse their influence on the catheter simulation process and eventually to improve the simulation. An improvement of the simulation is verified by a lower average Euclidean distance value between the real catheter path and the simulated catheter path. If the curvature minimising approach used in this thesis to simulate a catheter proves to be close to the real catheter shape, the parameters are adjusted to achieve the lowest average Euclidean distance value and therefore the closest approximation. The parameters that influence the optimiser are called:

- Maximum Evaluation
- Maximum Optimiser Iteration
- Minimum Improvement

In the following, all these parameters are explained in detail in order to provide an understanding of their influence on the accuracy of the catheter simulation and thus their importance for the optimisation process.

1. First, maximum evaluation. As mentioned previously the curvature minimising catheter path is calculated by using an optimiser that repeatedly evaluates different catheter paths. Maximum evaluation limits the amount of evaluations the optimiser can utilize. For every quadratic approximation utilized by the Newton optimiser a set number of evaluations is needed. Therefore, limiting the total number of evaluations limits the total number of iterations that can be performed which constrains the computational time of the simulation.
2. The second parameter is maximum optimiser iteration which is connected with maximum evaluation. It limits the number of iterations the optimiser can perform. Each iteration process results in an approximation of a quadratic function. The minimum of this quadratic function is then used as a new optimal value. Limiting this value reduces the computational time by limiting the amount of iterations the optimiser can calculate. For each iteration, one quadratic approximation is necessary that needs a certain number of evaluations.
3. Third, minimal improvement. Minimal improvement is a parameter that is used to terminate the optimiser if the improvement (measured by the sum of curvatures comparatively) between two iterations is smaller than a value  $X$ . It therefore terminates the optimiser. At a certain point the improvement will be so small that any additional computational strain is not justified and therefore it stops the vessel path to catheter path simulation process. The currently obtained curvature minimising catheter path will be considered to be the optimal.

Each of these three parameters constrain the optimiser. Reaching the limit of allowed evaluations or iterations stops the optimisation process. The process is terminated when the minimum improvement value is not met, as well. The aim is to set these parameters to a value such that the average Euclidean distance values converges, while



simultaneously maintaining a computational strain within reason. Although exact computational time is not analysed in this thesis, an overall reduction is desirable.

Apart from the optimiser parameters, there are two influence factors that are analysed as well. The influence of the sampling distance on the curvature of the final calculated catheter path and the influence of different mechanical forces applied on the original catheter path with respect to the simulation accuracy.

## 6.2 Additional Influence Factors analysed in this Thesis

In the following chapter, additional influence factors, are considered. They do not have a direct influence on the optimisation process, but nevertheless have the potential to improve the overall simulation approach as well as to reduce the computational strain on the system.

### 6.2.1 Sampling Distance in Relation to Curvature

The sampling distance is an influence factor, that is analysed in this thesis, however, it is not set inside the optimiser itself. In this case, the impact of varying sampling distances on the curvature of the calculated catheter path is analysed. It is important to note that the final IntelliCath navigation system compares curvature data. Therefore, the impact of sampling on the curvature of a simulated catheter path is studied. This is done by using the previously calculated vessel graphs. These graphs are then transformed into catheter paths and their curvature is measured throughout each data point. Visualising the curvature composition of each case with varying sampling distances illustrates the impact it has on the overall curvature value of each catheter.

### 6.2.2 Influence of Mechanical Forces on the Curvature of the Catheter

As mentioned in chapter 5, subsection 5.3, there is an additional set of eight recordings provided to further evaluate the simulation approach to represent a catheter path through a vessel system. The use of the recordings has a unique benefit compared to the other image data sets; the advantage of being able to visualise movement. Each recording

consists of a multitude of frames. These frames can be used to visualise the differences in accuracy of the vessel path to catheter path simulation in terms of pushing and pulling the original catheter. Selecting frames of a catheter within one vessel branch and choosing the corresponding frames based on pushing or pulling the catheter, made assessing the impact of these forces on the accuracy of the simulation approach possible. This is done by using the provided catheter extraction network that can extract a catheter from any selected frame in the recording. Using the extracted real catheter path and comparing it to the simulated catheter path for the corresponding vessel branch, made the comparison between pushing and pulling a catheter, by using the corresponding average Euclidean distance, possible. With this the accuracy of the catheter path simulation approach with regards to different mechanical influences is analysed.

### 6.3 Euclidean Distance Calculation

As mentioned throughout this thesis, the Euclidean distance calculation is the base parameter for evaluating the success of the simulation approach. Each set of sampled real and calculated catheter paths are compared to each other. Each marker position extracted from the real catheter path is compared with the closest marker position from the calculated catheter path. Each time calculating the Euclidean distance value for the corresponding marker. The mean distances taken by this value represent the average distance between the two overlapped catheter paths.

It is crucial to mention that for this comparison to be successful, the reference list (in this thesis the real catheter path must have fewer marker points than the other list. Conversely, this means that the calculated catheter path must have much more markers. As represented in figure 24.

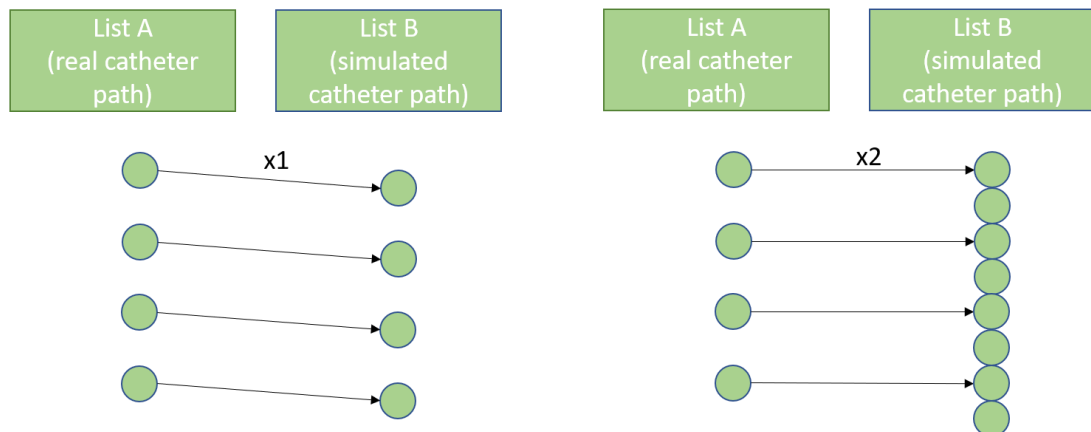


Figure 24: Visualisation of Euclidean distance calculation for an insufficiently sampled simulated catheter path (left) and a sufficiently sampled simulated catheter path (right). B-Spline interpolation is used to increase the number of data points in the comparing list. Length of  $x_1$  is different from  $x_2$ .

Having numerous data points in the simulated catheter path, enables each marker position in the reference list to have a corresponding marker in the other list. Therefore, increasing the marker points of the simulated catheter path is necessary to avoid the calculation of false Euclidean distance values. This is achieved by interpolating each calculated catheter path after its creation by using a B-spline interpolation method. This method is capable of accurately describing the space between each data point, as mentioned in chapter 3, subsection 3.5, and helps decreasing the sampling distance of the created catheter path. The value for the interpolation is set to a factor of 0,25, which effectively increased the amount of data points in the simulated catheter path drastically. This ensured, that the reference list always has a data point from the corresponding list close enough for accurate comparison. Using this interpolation method after the catheter path creation process, is necessary, as using it beforehand would result in a diminution of the output of the Newton optimiser as mentioned in chapter 6, subsection 6.1. The added markers proved to be efficient representations of added data positions as they do not change the shape of the catheter. By eliminating excess data points and interpolating the simulated catheter path, the errors in the Euclidean distance calculation can be eliminated. Therefore, the mean value is capable to represent the distance between the calculated catheter path compared to the real catheter path.

## 6.4 Evaluation Network

In this chapter, the functionality of the evaluation network is presented, which is used to calculate the overall average Euclidean distance.

The evaluation network is the last network building block of this thesis. It combines all segmented images and uses vessel path to catheter path simulation and overlapping to calculate an overall average Euclidean distance value. This network initially loads both the centre line representation of the vessel graph and the sampled real catheter path. It then proceeds to change the vessel path into a catheter path using a previously chosen set of values for maximum evaluation, maximum optimiser iteration and minimum improvement as basis for the simulation algorithm. After generating the simulated catheter path, it interpolates and then overlaps the simulated and the real catheter. It then uses the intersection area of both bounding boxes to cut out excess data points. This was only possible for the recordings, as explained in chapter 5, subsection 5.5. For the other cases the margin adjustment is performed manually as described in chapter 5, subsection 5.5. Then the simulated catheter path and the real catheter path are compared to each other by calculating their average Euclidean Distance value. These calculation steps are carried out consecutively for each image data set. Each time the resulting corresponding average Euclidean distance value is saved for every case along with the corresponding parameter setting in a separate list.

## 6.5 Iterations

A core factor of parameter optimisation is the iteration process. After creating the final evaluation network, that can calculate the average Euclidean distance error of both catheter paths for multiple data sets, the topic of iteration becomes important. The idea is to put the evaluation network into a loop and to change one of the three mentioned optimiser parameters in predefined steps. Performing multiple iterations with one changing parameter value is necessary to determine their influence on the accuracy of the simulation. This method is also used to determine the optimal parameter setting that approaches the final convergence value in shortest time. For each of the three parameter values that are changed, a graph is generated, that represented the corresponding change of the overall average Euclidean distance through each iteration.

## 7 Results of the Optimisation

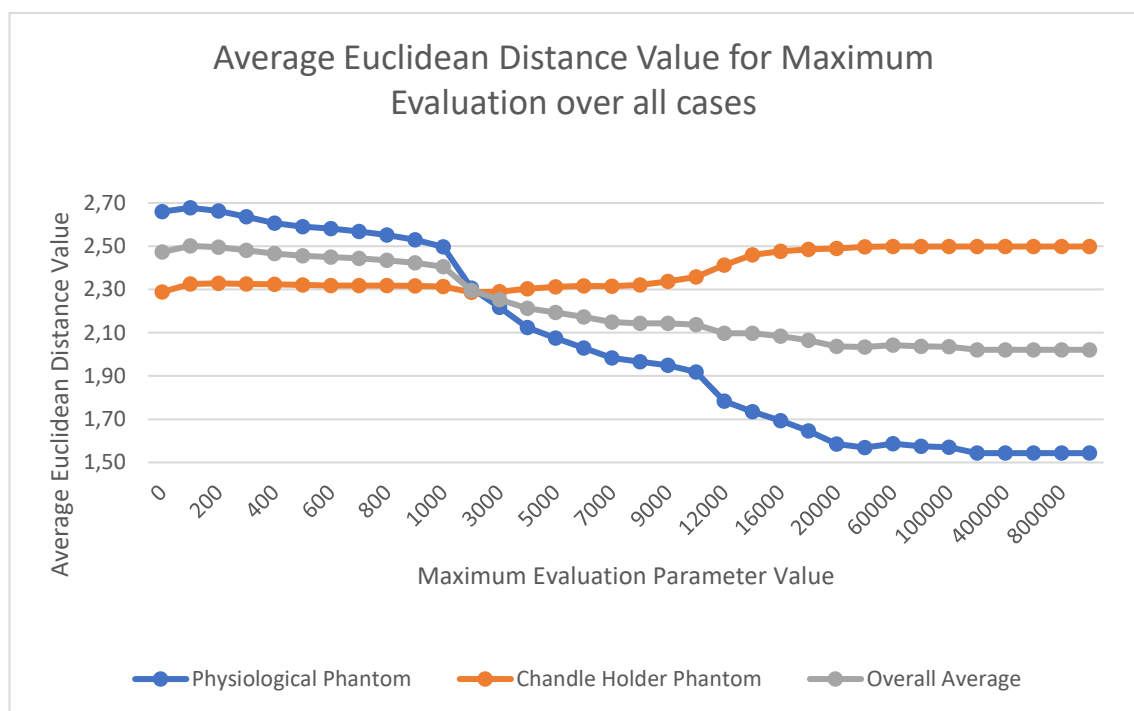
This chapter focuses on the summary and presentation of the gathered results from use of the developed evaluation network described in the previous chapters. The parameters maximum evaluation, maximum optimiser iteration and minimum improvement are all analysed in a similar way. Each of these parameters is changed gradually from a value 0 up to a value of 1.000.000 while the step size is changing accordingly like it is shown in the table 1:

Value of the parameter	Step size
0-1000	100
1000-10000	1.000
10000-20000	2.000
20.000-100.000	20.000
100.000-200.000	100.000
200.000-1.000.000	200.000

Table 1: Parameter step sizes of the three simulation parameters, used for the evaluation.

This step size is used for the maximum evaluation and maximum optimiser iteration. The parameter for the minimum improvement is treated differently, as its value is calculated by the formula “1/h”, where “h” represents the step size given in table 1. The output for a parameter value of 0 is calculated separately and implemented afterwards for the minimum improvement parameter. Each iteration loop has always one parameter that is continuously changed and two parameters that are either set to a value of  $10^6$  for maximum evaluation and maximum optimiser iteration or to a value of 0 for minimum improvement. This is necessary to prevent the other two parameters from terminating the one that is currently analysed. Setting these values sufficiently high or low, erases the influence of other parameters interfering with the calculation at first. Therefore, the output can be traced back directly to the influence the currently analysed parameter has on the overall evaluation network. Even though the parameter of minimum improvement is set to a value of 0 and therefore should never stop the optimisation of the simulated catheter path unless the other parameters reach their maximum values, this parameter nevertheless terminates the calculation at a high level of convergence. Since the reduction of curvature of the newly created catheter path compared with the current optimal value is less than a certain precision. Hence, the algorithm saves it as zero instead and therefore the optimisation is terminated. Still a significant trend in parameter

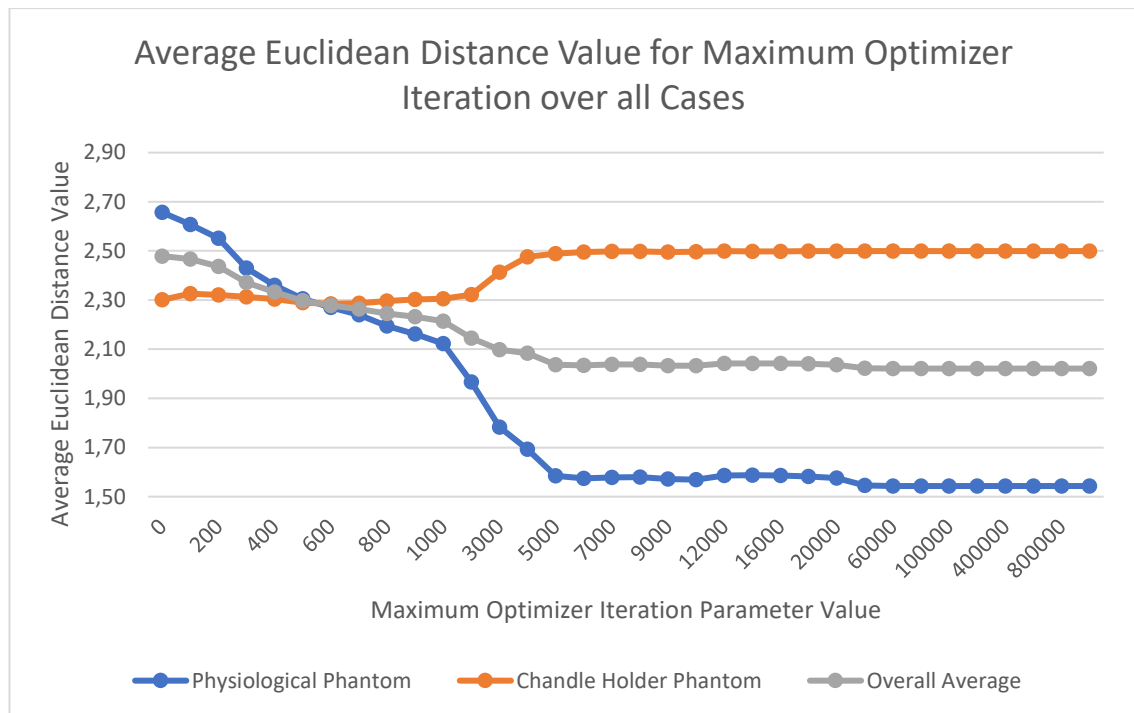
changes is visible. Furthermore, since the curvature minimising process is stopped by a minimum improvement value of 0, it can be assumed that the improvement of the newly created catheter path is insignificant in terms of curvature minimisation. This is also reflected by the second and the last average Euclidean distance values for each case listed in the Appendix. The last two minimum improvement parameter values are  $1 \cdot 10^{-6}$  and 0. The changes in the average Euclidean distance between these two are for all cases ranging values between  $1 \cdot 10^{-4}$  mm to  $4 \cdot 10^{-3}$  mm, thus confirming up the previously made assumption. It is important to mention that the evaluation results showed drastically changing Euclidean distance values for the cases. As a consequence of this, the representation as an average over all cases deemed to be insufficient. The data suggested a separation between the physiological vessel representations (cases 1-4, which are represented in blue in graph 1) and the candle holder phantom (cases 5-8, which are represented in orange in graph 1).



Graph 1: Average Euclidean distance value over changing maximum evaluation parameters. Separated from cases 1-4 (physiological vessel representations) and 5-8 (candle holder phantom).

For maximum evaluation, graph 1 shows that the physiological vessel systems (cases 1-4) show an overall decrease in the average Euclidean distance value for increasing parameter values. Starting at a value of 2,660 mm and ending at a value of 1,543 mm, which correspond to a reduction of 41,99 %. The candle holder phantom increased from

a value of 2,288 mm to 2,499 mm which is an increase of 9,22 %. Both curvatures indicate a flattening average Euclidean distance value with increasing parameter values.



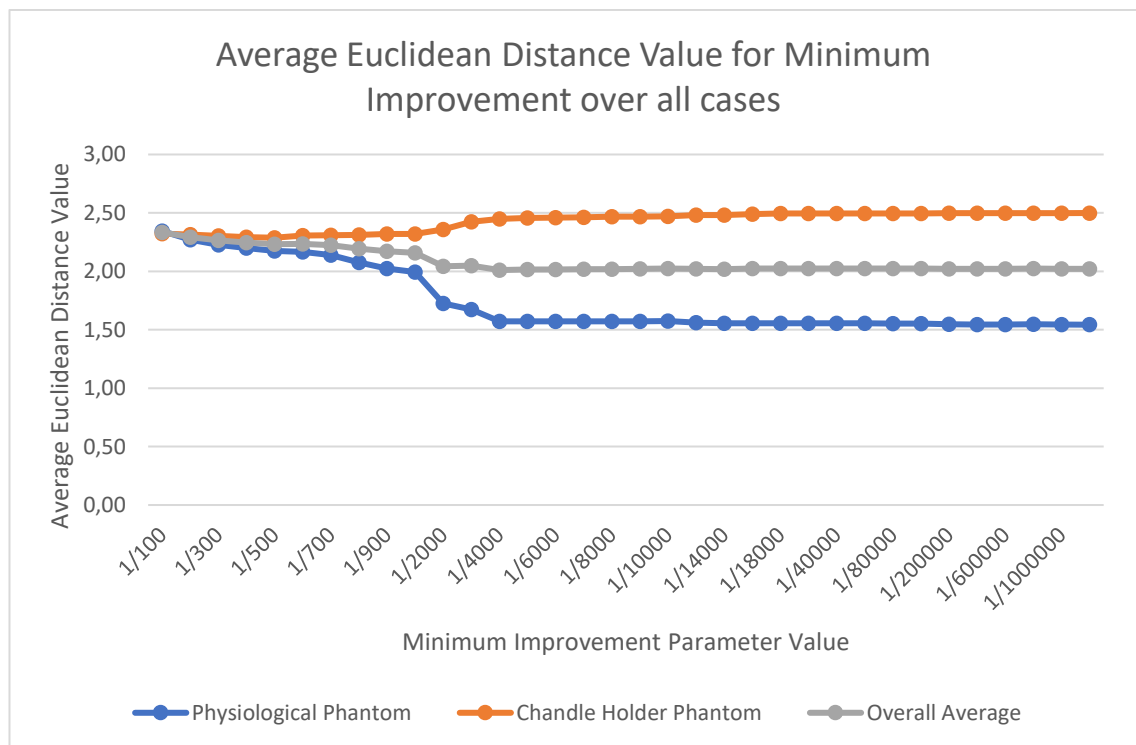
Graph 2: Average Euclidean distance value over changing maximum optimiser iteration parameters. Separated from cases 1-4 (physiological vessel representations) and 5-8 (candle holder phantom).

For maximum optimiser iteration, the overall average Euclidean distance value for the physiological vessel representation and the candle holder phantom showed similar behaviour compared to the average Euclidean distance value of the maximum evaluation parameter.

The average Euclidean distance value for the physiological vessel system is ranging between a value of 2,657 mm and a value of 1,543 mm which correspond to a decrease of 41,92 %. The candle holder phantom starts at an average Euclidean distance value of 2,301 mm and ends at a value of 2,499 mm which is an increase of 8,61 %.

This similarity is due to the start and end value of these parameters. At the beginning it starts with a maximum evaluation value of 0, which implies that the quadratic function approximation of the Newton optimiser is not able to approximate a quadratic function, due to the lack of evaluations. Also, by setting the maximum optimiser iteration value to 0, the program isn't able to utilize the Newton optimiser process as well, which means that both starting values are identical. Cases where the starting value is different, are explained by the manual list adjustment. However, the differences are so small, ranging in the magnitude of hundredths of millimetres, that the values can be considered to be

identical for further analysis. The similarity of the last values can be explained by the parameter settings. In the end both values for both parameter evaluations have a value of 1.000.000, which makes them have the same average Euclidean distance value. What differs however is the velocity at which both parameters achieve a point of convergence.



Graph 3: Average Euclidean distance value over changing minimum improvement parameters. Separated from cases 1-4 (physiological vessel representations) and 5-8 (candle holder phantom).

The minimum improvement value starts for the physiological vessel representation at a value of 2,344 mm and end at a value of 1,543 mm, corresponding to a decrease of 34,17 % over all parameter values. The candle holders starting value is 2,323 mm and the final value is 2,500 mm, therefore resulting in an increase of 0,177 mm corresponding to an increase of 7,62 %. Seeing the result and the differences in behaviour based on the analysed case, it is advisable to visualise the image data case by case to improve the validity of the final conclusion, by knowing the exact data constellation of the resulting overall average Euclidean distance value.



## 7.1 Physiological Vessel Phantoms

A separation of the cases into physiological vessel representations and candle holder phantom, resulted in twelve different data sets for each the physiological vessel phantom and the candle holder respectively. To maximise clarity the starting position as well as the ending positions and the general increase or decrease in the overall average Euclidean distance value as well as the value at which the data approaches near the convergence (near here means that the overall behaviour of the data changes only marginally in value compared to the rest of the data, since the amount of change differs from case to case. Connecting this behaviour to a set value would be less efficient) is visualised in the following table. The corresponding data are listed in the appendix.

Maximum Evaluation

Case	Starting Value [mm]	Final Value [mm]	Difference [mm]	Convergence, approached at [Parameter Value]
1	1,7773	1,2320	0,5453	4.000
2	2,2614	1,5084	0,7530	200.000
3	4,7092	2,0878	2,6214	20.000
4	1,8935	1,3446	0,5489	40.000

Table 2: Start and end value of the average Euclidean distance for the maximum evaluation parameter, for cases 1-4. The value at which the data approaches convergence is listed as well.

Maximum Optimiser Iteration

Case	Starting Value [mm]	Final Value [mm]	Difference [mm]	Convergence, approached at [Parameter Value]
1	1,7773	1,2320	0,5453	2.000
2	2,2614	1,5084	0,7530	40.000
3	4,6949	2,0878	2,6071	5.000
4	1,8935	1,3446	0,5489	6.000

Table 3: Start and end value of the average Euclidean distance with varying maximum optimiser iteration parameter, for cases 1-4. The value at which the data approaches convergence is listed as well.

### Minimum Improvement

Case	Starting Value [mm]	Final Value [mm]	Difference [mm]	Convergence, approached at [Parameter Value]
1	1,7912 (at 1/10)	1,2320	0,5592	1/70
2	2,2659 (at 1/10)	1.5084	0,7575	1/200
3	4,6925	2,0878	2,6047	1/4.000
4	1,8024	1,3446	0,4578	1/12.000

Table 4: Start and end Value of the average Euclidean distance with varying minimum improvement parameter, for cases 1-4. The value at which the data approaches convergence is listed as well.

Each of the four physiological vessel representations show a decrease of the average Euclidean distance with increasing parameter values. Furthermore, the parameter values at which the cases approach the final convergence differ. Maximum evaluation approaches convergence at an average value of 66.000, maximum optimiser iteration at an average value of 13.250 and minimum improvement at  $19,619 \cdot 10^{-3}$ . A slight change in the parameter for the minimum improvement parameter slightly resulted in the fastest approach to convergence for case 1 in this thesis, at a value of 1/40, which is lower than the set starting position for minimum improvement at 1/100. Case 2 shows increased parameter values for maximum evaluation and maximum optimiser iteration comparatively, therefore the average is increased.

## 7.2 Candle Holder Phantom

### Maximum Evaluation

Case	Starting Value [mm]	Final Value [mm]	Difference [mm]	Convergence, approached at [Parameter Value]
5	1,8353	2,1349	0,2996	40.000
6	1,8047	2,3328	0,5281	40.000
7	2,9794	3,0911	0,1117	40.000
8	2,5322	2,4373	0,0949	40.000

Table 5: Start and end value of the average Euclidean distance with varying maximum evaluation parameter, for cases 5-8. The value at which the data approaches convergence is listed as well.

### Maximum Optimiser Iteration

Case	Starting Value [mm]	Final Value [mm]	Difference [mm]	Convergence, approached at [Parameter Value]
5	1,8884	2,1349	0,2465	6.000
6	1,8047	2,3328	0,5281	6.000
7	2,9794	3,0910	0,1116	5.000
8	2,5322	2,4373	0,0949	7.000

Table 6: Start and end value of the average Euclidean distance with varying maximum optimiser iteration parameter, for cases 5-8. The value at which the data approaches convergence is listed as well.

### Minimum Improvement

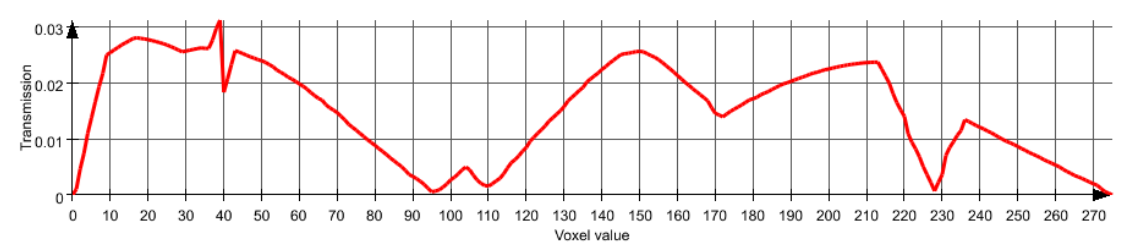
Case	Starting Value [mm]	Final Value [mm]	Difference [mm]	Convergence, approached at [Parameter Value]
5	1,9089	2,3150	0,4061	1/16.000
6	1,8186	2,3328	0,5142	1/12.000
7	3,0137	3,0910	0,0773	1/5.000
8	2,5521	2,4373	0,1148	1/7.000

Table 7: Start and end value of the average Euclidean distance with varying minimum optimiser parameter, for cases 5-8. The value at which the data approaches convergence is listed as well.

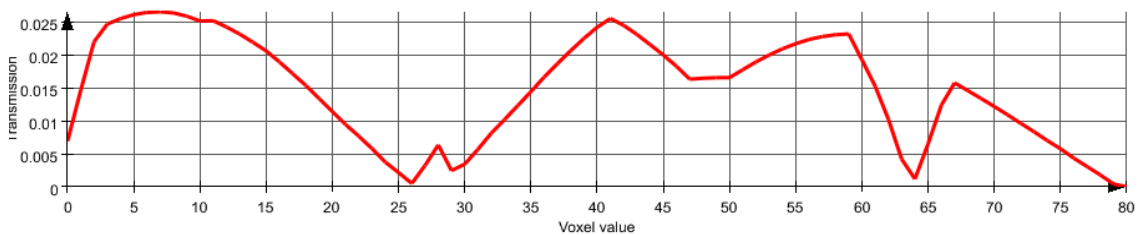
Three out of four data sets increase in average Euclidean distance value with increasing parameter settings. Case 8 is the only data set that decreases when, comparing the start and end value. Cases 5 and 7 show a slight decrease at first, but then proceed to increase again and converge at a value higher than at the beginning. Case 8 shows a short peak after a period of decreasing values which then proceeds to decrease again, resulting in an average Euclidean distance value decrease overall. Case 6 is steadily increasing with increasing parameter values. The influence of the parameters on the end results remain analogue to the physiological vessel system, with the highest average convergence value of 40.000 for the maximum evaluation parameter, 6.000 for the maximum optimiser iteration parameter and  $1,222 \cdot 10^{-4}$  for the minimum optimiser parameter.

### 7.3 Other Analysed Parameters

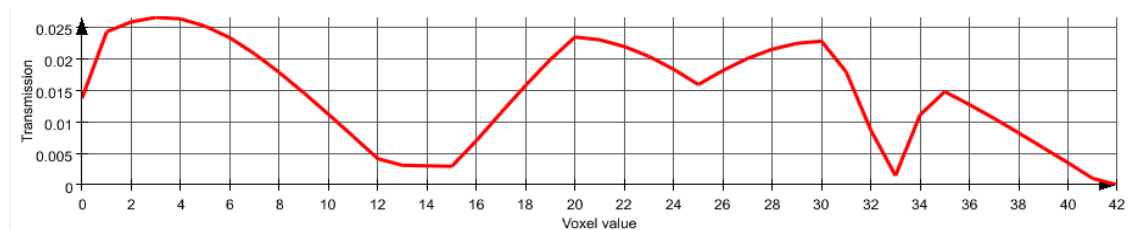
In addition, to the average Euclidean distance value of all phantoms, the sampling distance is analysed, to visualise possible changes in the curvature of the simulated catheter in relation to the sampling.



Graph 4: Curvature representation of a catheter path for a sampling distance of 1 mm. The transmission is represented against the voxel value.



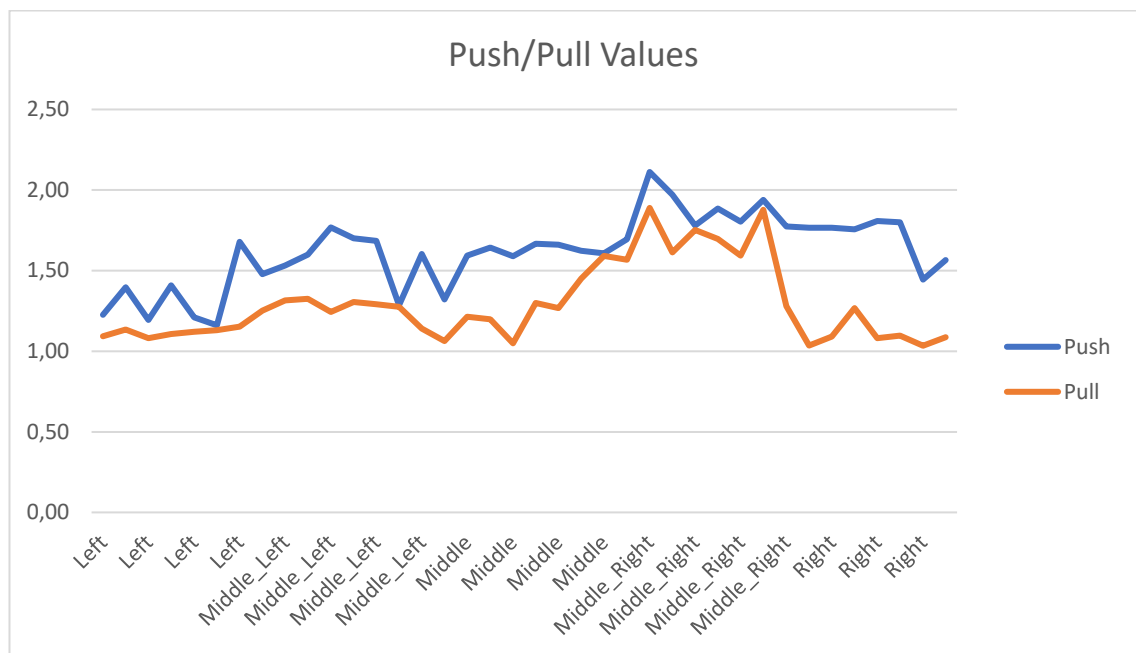
Graph 5: Curvature representation of a catheter path for a sampling distance of 5 mm. The transmission is represented against the voxel value.



Graph 6: Curvature representation of a catheter path for a sampling distance of 10 mm. The transmission is represented against the voxel value.

Graphs 4, 5 and 6 show that the sampling distance has only marginal effect on the curvature distribution of the simulated catheter path. All three sampling distances from 1 mm over 5 mm up to 10 mm have similar curvature distributions.

Finally, the recordings are used to analyse the accuracy of the optimisation approach with regards to pushing and pulling forces by selecting different frames representing each case. Using this method and applying it on each vessel branch in the phantom for every recording shows the impact of mechanical influence on the simulation accuracy as shown in graph 7.

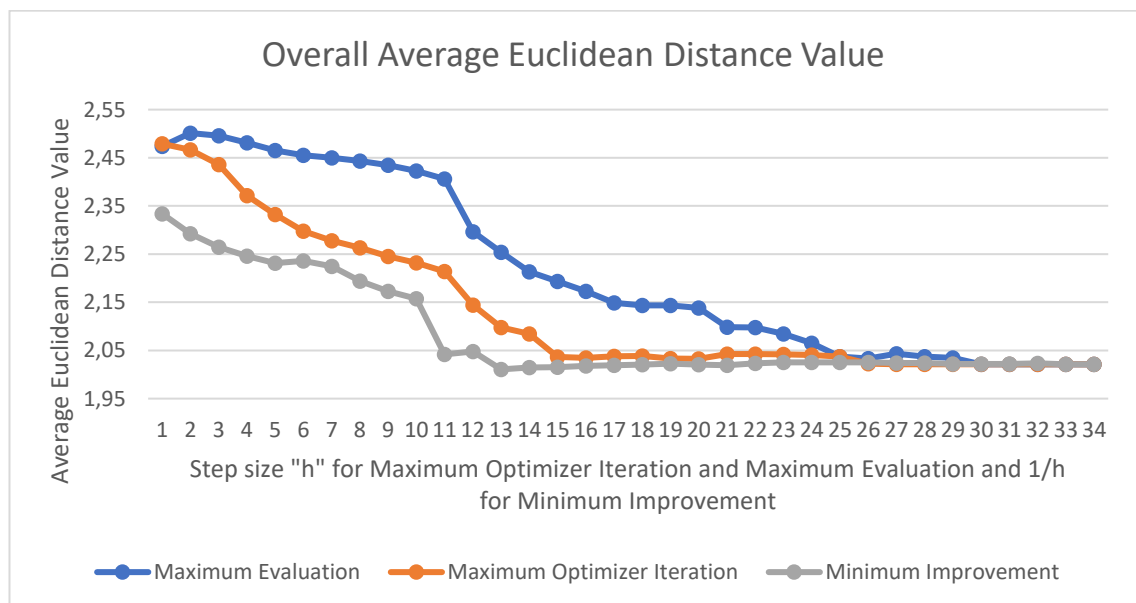


Graph 7: Influences of pushing and pulling a catheter in a vessel system on the accuracy of the catheter simulation.

All analysed frames show lower average Euclidean distance values for the pulling case.

## 8 Discussion

In the following chapter the validity and the information value of the currently provided optimisation data is analysed and discusses. This serves the purpose of evaluating this data based on the procedure it was detected as well as discuss probable shortcomings of the detected information. Starting with a general analysis of the overall average Euclidean distance value behaviour and then proceeding to divide the physiological vessel and the candle holder. Following up with possible explanations on why the values behave in such way and ending with implementing the information's drawn from the additionally analysed parameters. The influence each parameter has on the optimisation process is similar in all cases. Maximum optimiser iteration and minimum improvement turned out to be parameters that approach the convergence value much faster than the maximum evaluation parameter as shown in graph 8.



Graph 8: Average Euclidean distance value for all parameters of the simulation over all cases and parameter values.

As discussed in this thesis, the improvement in terms of closeness to reality provided by the underlying optimisation process varies depending on the case that is analysed. As previously shown, the physiological vessel representations do improve significantly by about 41,99 % with maximum evaluation, 41,92 % for maximum optimiser iteration and 34,17 % for minimum improvement, with increasing parameter values. Here the curvature minimising approach seems to be well adjusted in simulating the curvatures of a catheter inside a vessel system.

In contrary to that, the candle holder cases do not seem to benefit from the curvature minimising approach. This results in an average Euclidean distance value increase of 9,22 % for the maximum evaluation, 8,61 % for the maximum optimiser iteration and 7,62 % for minimum improvement. Here, the curvature minimising approach seems to suffer from other influence factors diminishing the outcome. It is interesting to note that only the candle holder phantom shows such behaviour. The physiological vessel representations consist of three completely different vessel constellations, and they all illustrate a decrease of the average Euclidean distance. Even the Euclidean distance value decrease in case 8 is vanishingly low with an improvement of only 0,09 mm to 0,12 mm, depending on the parameters changed, compared to the improvement of cases 1-4.

A Possible explanation for the lack of improvement in the candle holder phantom is, that the connections between vessel branches had to be implemented manually, as they are not visible in the CT images. The assumption was, that the connections have the same diameter as the rest of the phantom. It was later shown that the radius of the connecting pieces of the candle holder were smaller in diameter than the rest which leads to changing the movement of the catheter. Implementing the change in diameter could improve the optimisation result. Also, it is possible, that the optimiser is well adjusted for approximating curvature minimising movement through short intervals with rapid changes in curvature values. The candle holder phantom consisted of large tubular structures with only a few rapidly changing curvature values compared to the other phantoms used in this thesis. Mechanical influences also play a more important role with rising catheter length. Having a comparatively long vessel system with long tubular structures compared to the physiological vessel phantom, increases the influence of friction and bending forces applied on the catheter. This statement will be further elaborated in the analysis of the recordings.

Finally, it was discovered that small changes in diameter of the vessel graph conclude to significant changes in the output of the average Euclidean distance value. Case 8 was analysed on this matter exemplary. The segmented vessel graph from case 8 seemingly has a smaller diameter than the vessel system would suggest. By applying a dilation and filling areas with "CreateObject" the overall diameter of the vessel graph was increased to represent the inner vessel system accurately. This increase in diameter resulted in a change in average Euclidean distance value, presented in table 8-9:



Parameter value for maximum evaluation and maximum optimiser iteration	Vessel graph without increased diameter [mm]	Vessel graph with increased diameter [mm]	Difference [mm]
0	2.5322	2,2544	0,2778
1.000.000	2.4373	1,9267	0,5106

Table 8: Changes between the average Euclidean distance values with increased vessel diameter, for maximum evaluation and maximum optimiser iteration.

Parameter value for minimum improvement	Vessel graph without increased diameter [mm]	Vessel graph with increased diameter [mm]	Difference [mm]
1/1.000.000	2,5521	2,1395	0,4126
0	2,4373	1,9268	0,5105

Table 9: Changes between the average Euclidean distance value with increased vessel diameter, for minimum improvement.

The tables represent the impact the vessel graph modification of case 8 has on the overall evaluation. It can be concluded that modifications in the vessel graph can result in significant changes in the simulation. Precise segmentation is therefore required to ensure a reliable evaluation result.

Tracking the curvature of a calculated catheter path by using different sampling distances was a significant gain. As shown in graph 4-6, the curvature seems to change only slightly with decreasing sampling distances, therefore the accuracy of the navigation approach is not significantly reduced. This could lead to lowering the computational strain on the system dramatically. Nevertheless, a concrete analysis of the exact changes in curvature over varying sampling distances would be helpful to substantiate this claim and would help to further specify the exact impact of the sampling distance numerically.

Finally, the difference between pushing and pulling forces, derived from the recording provided in this thesis is analysed. These results show a discrepancy between the accuracy of the simulation module based on the mechanical force the real catheter is experiencing. At this point it is important to point out that the recordings, as mentioned in chapter 5, subsection 5.5, have two-dimensional bounding boxes and therefore no informational value in z-direction. It is possible, that the information obtained by including the z-direction would lead to a different outcome. However, assuming that the impact in z-direction is only marginal, the following statements can be drawn, due to the limited movement within the tubular vessel system in z-direction. It seems that the simulation

module is more accurate in representing catheters experiencing pulling forces. This leads to the conclusion that the simulation module should be expanded by implementing mechanical influences into the calculation. These influences could include the prediction of the bending behaviour of catheters made of a certain material and friction forces which also play a role in the movement of the catheter. It can be expected that the implementation of these external mechanical forces into the simulation could improve the algorithm tremendously. Moreover it could not only increase the improvement of the cases that are already benefitting from the parameter optimisation, it could also start lowering the distance value of the cases on which the optimisation had only marginal impact, such as the candle holder.

## 9 Conclusion

The aim of this chapter is to provide a cohesive conclusion of all results identified in this thesis. The evaluation of the curvature minimising approach leads to the conclusion that it is a sufficient approach to simulate the behaviour of a catheter within a physiological vessel system. Nevertheless, it must be mentioned that the candle holder cases in this thesis showed negative results. Although they were minimal compared to the improvement of the other cases, they still need to be addressed. As discussed in chapter 8, including mechanical influences could lead to an improve of the overall accuracy of the system by implementing factors like friction, material and therefore bending behaviour of the catheter.

Furthermore, precise segmentation is needed for reliable results as well. Changing the vessel graph diameter resulted in drastic changes in the simulation and therefore the average Euclidean distance values of the candle holder. Therefore, it can be concluded that the simulation is very dependent on segmentation. This is a key factor that should be kept in mind. Automatising the segmentation algorithm could help improve the results and avoid strong average Euclidean distance value changes due to having consistent and reliable segmentation procedures and results.

As shown in this thesis, especially the change of the parameters maximum optimiser iteration and minimum improvement are the fastest way to arrive at a converging value. In order to achieve these results quickly, the other values have to be set to a value that keeps them from terminating the calculation as much as possible. Based on the information drawn in this thesis, averaging all parameter settings for each case at which they arrive at near convergence, results in the following parameter recommendations represented in table 10.

Parameter	Averaged Value
Maximum Evaluation	53.000
Maximum Optimiser Iteration	9.625
Minimum Improvement	$2,513 \cdot 10^{-3}$

Table 10: Parameter recommendations for the catheter simulation derived from the generated Euclidean distance data.

These recommendations are only shown to give a general overview of the relation each value has to the other. It gives an idea of how the parameters should stand in proportion to each other. Every vessel system has a different set of optimal values. This argument

is further supported by the higher values for maximum evaluation and maximum optimiser iteration for case 2 comparatively as well as the varying values for minimum improvement over all cases. Nevertheless, the relation of each parameter to each other is the same. A sufficiently high number of evaluations for the Newton optimisation process, is necessary to give the optimiser the possibility to arrive at a number of iterations that leads to convergence. Setting the minimal improvement value to a significantly low value, additionally helps simulating a final curvature minimising catheter path.

The informational value gained from varying the sampling distance was significant. The computational strain on the system can approximately be lowered significantly, by using a higher sampling distance due to its low impact on the curvature function. In addition, the information gained from the recordings also has drastic impact on the future of this catheter navigation approach. It supports the argument that the implementation of multiple mechanical parameters into the system could lead to a significant improvement of this system.

In summary, the underlying curvature minimising approach of the IntelliCath catheter navigation system has the potential to be an adequate method of portraying catheter movement inside a vessel. Further implementing mechanical influences and as a result of that implementing more parameters into the catheter path simulation algorithm will surely lead to an even better approximation of movement and therefore an even better catheter navigation approach.

## 10 Outlook

The IntelliCath approach of anticipating the movement of a catheter within a vessel, by approximating a curvature minimising path, seemed to be highly applicable for certain cases. As suggested in this thesis, there seem to be mechanical influences that should be implemented into the algorithm to further improve the system and analyse its accuracy.

Using the evaluated data sets that were calculated in this thesis as reference to measure the improvement of the simulation after mechanical influences have been implemented would be of great value. Nevertheless, the current predictions show a great amount of potential.

Additionally, extending the evaluation approach on various vessel systems, with varying shapes and sizes, would improve the evaluation even further. Due to the different vessel systems possible difficulties or issues in the simulation could be detected that were not visible in this thesis.

Automatising the segmentation process for the optimiser would be beneficial as it was concluded that low changes in diameter of the vessel graph resulted in a calculated catheter shapes that greatly differ from each other. On that topic, with an automatised segmentation network, the candle holder's vessel system could be segmented again, now with precise diameters for the vessel and connecting pieces. Automatisation would provide consistent and reliant segmentation data for the simulation.

Finally, the use of a different metric would be of great informational value. In this thesis the Euclidean distance value is used to measure the validity of the simulation approach. Since the IntelliCath catheter navigation project uses curvature data, the analysis of the curvature distance would be of great interest as well.

Extending on the deficits mentioned in this thesis and implementing different parameters and vessel environments would result in an, reliable and precise approach for catheter navigation. This system could represent a milestone in the future of endovascular navigation. When the developing process is finished it will improve the endovascular navigation and take a great burden off the shoulders of future clinical experts and as a consequence, minimising the health risks for patients.

## Bibliography

- Al-amri, S. S., Kalyankar, N. V., & Khamtikar, S. D. (2010, May). Image Segmentation by Using Threshold Techniques. *Journal of Computing, Volume 2 No. 5*, pp. 83-86.
- Anderon, P. L., Gelijns, A., Moskowitz, A., Arons, R., Gupta, L., Weinberg, A., . . . Kent, C. K. (2004, June). Understanding trends in inpatient surgical volume: Vascular interventions, 1980-2000. *Journal of Vascular Surgery, Volume 39 No. 6*, pp. 1200-1208.
- Bakos, J. D. (2016). *Embedded Systems ARM Programming and Optimization*. Waltham MA, USA: Elsevier Inc.
- Briand, T., & Monasse, P. (2018, July). Theory and Practice of Image B-Spline Interpolation. *Image Processing On Line, Vol. 8*, pp. 99-141.
- Chong, E. K., & Zak, S. H. (2001). *An Introduction To Optimization*. Canada: John Wiley & Sons Inc.
- Farber, R. (2011). *CUDA Application Design and Development*. Waltham MA, USA: Elsevier Inc.
- Feneley, R. C., Hopley, I. B., & Wells, P. N. (2015, June). Urinary catheters: history, current status, adverse events and research agenda. *Medical Engineering & Technology, Volume 39 No. 8*, pp. 459-470.
- Hedberg, H. (2008). Image Processing Architecture for Binary Morphology and Labeling. Thesis. Lund University, Sweden.
- Hossain, M., & Abufardeh, S. (2019, May). A New Method of Calculating Squared Euclidean Distance (SED) Using pTree Technology and Its Performance Analysis. *EPIC Series in Computing, Volume 58*, pp. 45-54.
- Hou, H., & Andrews, H. C. (1978, December). Cubic Splines for Image Interpolation and Digital Filtering. *IEEE Transactions on Acoustics, Speech and Signal Processing, Volume ASSP-26 No.6*, pp. 508-517.
- Ikonomakis, N., Plataniotis, K. N., & Venetsanopoulos, A. N. (2000, June). Color Image Segmentation for Multimedia Applications. *Journal of Intelligent and Robotic System, Volume 28*, pp. 5-20.
- Kanopolous, N., Vasanthavada, N., & Baker, R. L. (1988, April). Design of an Image Edge Detection Filter Using the Sobel Operator. *IEEE Journal of Solide-State Circuits, Volume 23 No. 2*, pp. 358-367.
- Luani, B., Rauwolf, T., Genz, C., Schmeißer, A., Wiemer, M., & Braun-Dullaues, R. C. (2019, June). Intracardiac echocardiography versus fluoroscopy for endovascular and endocardial catheter navigation during cryo-ablation of the slow pathway in AVNRT patients. *Cardiovascular Ultrasound, Volume 17 No. 1*, pp. 1-8.

- Mahesh, M. (2001, July). The AAPM/RSNA Physics Tutorial for Resident Fluoroscopy: Patient Radiation Exposure Issues. *Radio Graphics, Volume 21 No. 4*, pp. 1033-1045.
- MeVis Medical Solutions AG [a]. Retrieved September 2020, from <https://mevislabdownloads.mevis.de/>:  
<https://mevislabdownloads.mevis.de/docs/current/FMEstable/ReleaseMeVis/Documentation/Publish/ModuleReference/FastMorphology.html>
- MeVis Medical Solutions AG [b]. (2020). Retrieved Juli 2020, from [mevislab.de](https://www.mevislab.de/):  
<https://www.mevislab.de/>
- MeVis Medical Solutions AG [c]. Retrieved June 2020, from [mevislabdownloads.mevis.de](https://mevislabdownloads.mevis.de/):  
<https://mevislabdownloads.mevis.de/docs/2.5/MeVisLab/Standard/Documentation/Publish/ModuleReference/DtfSkeletonization.html>
- MeVis Medical Solutions AG [d]. Retrieved June, 2020, from [mevislabdownloads.mevis.de](https://mevislabdownloads.mevis.de/):  
<https://mevislabdownloads.mevis.de/docs/current/MeVisLab/Standard/Documentation/Publish/ModuleReference/Sobel3D.html>
- MeVis Medical Solutions AG [e]. (2020, May). Retrieved August 2020, from [mevislabdownloads.mevis.de](https://mevislabdownloads.mevis.de/):  
<https://mevislabdownloads.mevis.de/docs/current/MeVisLab/Resources/Documentation/Publish/SDK/KernelProgramming/ch01s02.html>
- Olufunke, R. V., & Olusegun, F. (2009, January). A Descriptive Algorithm for Sobel Image Edge Detection. *Proceedings of Informing Science & IT Education Conference (InSITE)*, pp. 98-107.
- O'Neill, B. (2006). *Elementary Differential Geometry Revised 2nd Edition*. Amsterdam, Boston, Heidelberg: Elsevier Inc.
- Pajot, H. M. (2002). *Analytic Capacity, Rectifiability, Menger Curvature and Cauchy Intergral*. Berlin Heidelberg: Springer-Verlage.
- Richling, B. (2006, November). History of Endovascular Surgery: Personal Accounts of the Evolution. *Neurosurgery, Volume 56 No. 5*, pp. S3-30-S3-38.
- Sengur, A., Guo, Y., Ustundag, M., & Alcin, Ö. F. (2015, June). A Novel Edge Detection Algorithm Based on Texture Feature Coding. *Journal of Intelligent Systems, Volume 24 No. 2*, pp. 235-248.
- Sreedhar, K., & Panlal, B. (2012, February). Enhancement of Images Using Morphological Transformations. *International Journal of Computer Science & Information Technology (IJCSIT), Volume 4 No. 1*, pp. 33-50.

## List of Figures

Figure 1: Centre line representation of a vessel system. At the bifurcations (circled in red) it can be observed that the curvature values are high. Image created by E. Schmidt using MeVisLab. ....	3
Figure 2: Filter application in digital image processing. Example provided by courtesy of Prof. Dr. Schiemann's lecture on Medical Image Processing at the University of Applied Sciences from summer semester 2019. ....	7
Figure 3: Erosion process visually illustrated. Here, black pixels have the value 1 and white pixels the value 0. Image provided by courtesy of Prof. Dr. Schiemann's lecture on Medical Image Processing at the University of Applied Sciences from summer semester 2019. ....	10
Figure 4: Dilation process visually illustrated. Here, black pixels have the value 1 and white pixels the value 0. Image provided by courtesy of Prof. Dr. Schiemann's lecture on Medical Image Processing at the University of Applied Sciences from summer semester 2019. ....	11
Figure 5: MeVisLab network [left]. Used for loading images with ImageLoad and viewing these images with View2D. ImageLoad panel [right], used to specify the data path that is loaded. Image created by E. Schmidt using MeVisLab. ....	17
Figure 6: Candle holder vessel phantom used in this thesis for cases 5-8. Consists of a catheter inside of tubular structures made out of silicone, representing a vessel system. Image created by E. Schmidt using MeVisLab. ....	20
Figure 7: Physiological vessel systems: Phantom 1; cases 1-2. Provided by the ARCANDIS GmbH, Germany. Image created by E. Schmidt using MeVisLab. ....	21
Figure 8: Physiological vessel systems: Phantom 2; case 3. Provided by the United Biologics Inc., U.S.A. Image created by E. Schmidt using MeVisLab. ....	22
Figure 9: Physiological vessel systems: Phantom 3; case 4. Provided by the United Biologics Inc., U.S.A. Image created by E. Schmidt using MeVisLab. ....	22
Figure 10: Camera recordings of a catheter moving inside an acrylic tubular structure. Used in this thesis for analysis of mechanical influences. Image created by E. Schmidt using MeVisLab. ....	23
Figure 11: Image data for catheter segmentation after threshold was applied and before applying Sobel to get clearer boarder separation. Image created by E. Schmidt using MeVisLab. ....	25



Figure 12: Image data after applying Sobel for better separability between catheter and access data points. Image created by E. Schmidt using MeVisLab.....	25
Figure 13: Segmented catheter mask representing the catheter located in the image data, respectively. Later sampled and used as the real catheter path for the evaluation process. Image created by E. Schmidt using MeVisLab.....	27
Figure 14: Segmented catheter path after sampling. Each point represents one marker position in the generated XMarkerList. Image created by E. Schmidt using MeVisLab. ....	28
Figure 15: CreateObject interface for generating three-dimensional structures inside the vessel. Image created by E. Schmidt using MeVisLab.....	29
Figure 16: Skeletonized vessel graph representation of the candle holder image. The skeletonized vessel graph representation is not smooth and shows additional data points that need to be excluded for accurate vessel graph to catheter path simulation. Image created by E. Schmidt using MeVisLab.....	32
Figure 17: Candle holder centre line of the segmented vessel graph. Image created by E. Schmidt using MeVisLab. ....	33
Figure 18: Candle holder vessel graph after graph manipulation. Only vessel branch in which the catheter is located is left. Image created by E. Schmidt using MeVisLab. ...	33
Figure 19: Aorta vessel phantom (left) and, extracted inner Vessel Structure (right). Used for vessel segmentation. Images created by E. Schmidt using MeVisLab.....	36
Figure 20: Physiological vessel phantom (left) and extracted inner vessel structure (right). Used for vessel segmentation. Images created by E. Schmidt using MeVisLab. ....	36
Figure 21: Sampled catheter paths, real (left), simulated (right). Images created by E. Schmidt using MeVisLab. ....	37
Figure 22: Overlapped catheter paths. Visualizing different starting positions for each catheter path. As a result, start and end positions are cropped to align. Image created by E. Schmidt using MeVisLab. ....	38
Figure 23: Vessel graph to catheter path simulation. The red dots represent the inner vessel diameter and the green dots the centre line of the segmented vessel. The blue dots are the simulated catheter path. Extracted from MeVisLAB from the VesselGraphToCatheterPath help module.....	41
Figure 24: Visualisation of Euclidean distance calculation for an insufficiently sampled simulated catheter path (left) and a sufficiently sampled simulated catheter path (right).	

B-Spline interpolation is used to increase the number of data points in the comparing list.  
Length of x1 is different from x2..... 46

## List of Graphs

Graph 1: Average Euclidean distance value over changing maximum evaluation parameters. Separated from cases 1-4 (physiological vessel representations) and 5-8 (candle holder phantom). .....	49
Graph 2: Average Euclidean distance value over changing maximum optimiser iteration parameters. Separated from cases 1-4 (physiological vessel representations) and 5-8 (candle holder phantom). .....	50
Graph 3: Average Euclidean distance value over changing minimum improvement parameters. Separated from cases 1-4 (physiological vessel representations) and 5-8 (candle holder phantom). .....	51
Graph 4: Curvature representation of a catheter path for a sampling distance of 1 mm. The transmission is represented against the voxel value. Graph created by E. Schmidt using MeVisLab. ....	56
Graph 5: Curvature representation of a catheter path for a sampling distance of 5 mm. The transmission is represented against the voxel value. Graph created by E. Schmidt using MeVisLab. ....	56
Graph 6: Curvature representation of a catheter path for a sampling distance of 10 mm. The transmission is represented against the voxel value. Graph created by E. Schmidt using MeVisLab. ....	56
Graph 7: Influences of pushing and pulling a catheter in a vessel system on the accuracy of the catheter simulation. ....	57
Graph 8: Average Euclidean distance value for all parameters of the simulation over all cases and parameter values. ....	58

## List of Tables

Table 1: Parameter step sizes of the three simulation parameters, used for the evaluation. ....	48
Table 2: Start and end value of the average Euclidean distance for the maximum evaluation parameter, for cases 1-4. The value at which the data approaches convergence is listed as well.....	52
Table 3: Start and end value of the average Euclidean distance with varying maximum optimiser iteration parameter, for cases 1-4. The value at which the data approaches convergence is listed as well.....	52
Table 4: Start and end Value of the average Euclidean distance with varying minimum improvement parameter, for cases 1-4. The value at which the data approaches convergence is listed as well.....	53
Table 5: Start and end value of the average Euclidean distance with varying maximum evaluation parameter, for cases 5-8. The value at which the data approaches convergence is listed as well.....	54
Table 6: Start and end value of the average Euclidean distance with varying maximum optimiser iteration parameter, for cases 5-8. The value at which the data approaches convergence is listed as well.....	54
Table 7: Start and end value of the average Euclidean distance with varying minimum optimiser parameter, for cases 5-8. The value at which the data approaches convergence is listed as well.....	55
Table 8: Changes between the average Euclidean distance values with increased vessel diameter, for maximum evaluation and maximum optimiser iteration. ....	60
Table 9: Changes between the average Euclidean distance value with increased vessel diameter, for minimum improvement.....	60
Table 10: Parameter recommendations for the catheter simulation derived from the generated Euclidean distance data.....	62
Table 11: Average Euclidean distance value for maximum evaluation for all cases. ....	X
Table 12: Average Euclidean distance value for maximum optimiser iteration for all cases.....	XI
Table 13: Average Euclidean distance value for minimum improvement for all cases.....	XII
Table 14: Average Euclidean distance value for the recordings, while pushing the catheter.....	XIII
Table 15: Average Euclidean distance value for the recordings, while pulling the catheter.....	XIII

## List of Equations

Equation 1: Sobel operator decomposition. Extracted from (Bakos, 2016, p. 155). .....	8
Equation 2: Calculation of the gradient values for x and y direction. Extracted from (see Kanopolous, Vasanthavada, & Baker, 1988, p. 358). .....	8
Equation 3: Magnitude calculation for Sobel. Shows the elementwise combination of $G_x$ and $G_y$ to calculate the magnitude for each pixel. Approximated from (see Kanopolous, Vasanthavada, & Baker, 1988, p. 358), changing $E_H$ and $E_V$ to $G_x$ and $G_y$ . .....	8
Equation 4: Notation for erosion. Extracted from (see Hedberg, 2008, p. 33). .....	9
Equation 5: Notation for dilation. Extracted from (see Hedberg, 2008, p. 35). .....	10
Equation 6: Notion of the irreversibility of erosion and dilation. ....	11
Equation 7: Closing mathematically defined as dilation followed by erosion. Formula extracted from (see Hedberg, 2008, p. 36). .....	11
Equation 8: Euclidean distance calculation for distance between point p and q in $R^3$ . Extracted from (O'Neill, 2006, p. 44). .....	12
Equation 9 Spline calculation represented as “weighted sum of shifted normalized B-splines of order n”. Extracted from (see Briand & Monasse, 2018, p. 101). .....	12
Equation 10: Interpolation condition. Extracted from (Briand & Monasse, 2018, p. 101). .....	13
Equation 11: Calculation of Menger curvature using three non colinear points. Extracted from (Pajot, 2002, S. 29). .....	15

## Appendix

In this appendix the results of the Euclidean distance calculation, in form of a table for every case will be illustrated. These values conclude to the same result as represented in chapter 6 and following.

### Maximum Evaluation

Value	Case 1	Case 2	Case 3	Case 4	Case 5	Case 6	Case 7	Case 8
0	1.7773	2.2614	4.7092	1.8935	1.8353	1.8047	2.9794	2.5322
100	1.7929	2.2699	4.7178	1.9303	1.8932	1.8254	3.0152	2.5658
200	1.7840	2.2500	4.7049	1.9150	1.9057	1.8216	3.0168	2.5686
300	1.7607	2.2137	4.6947	1.8778	1.9049	1.8180	3.0146	2.5665
400	1.7171	2.1869	4.6849	1.8410	1.9003	1.8160	3.0140	2.5639
500	1.6954	2.1707	4.6690	1.8262	1.8943	1.8161	3.0126	2.5594
600	1.6897	2.1613	4.6552	1.8176	1.8875	1.8189	3.0132	2.5556
700	1.6847	2.1383	4.6396	1.8101	1.8850	1.8224	3.0142	2.5523
800	1.6829	2.0953	4.6239	1.8064	1.8834	1.8248	3.0140	2.5484
900	1.6750	2.0318	4.6089	1.8038	1.8813	1.8267	3.0127	2.5428
1000	1.6544	1.9410	4.5947	1.8014	1.8783	1.8281	3.0117	2.5370
2000	1.4352	1.6729	4.4100	1.7057	1.8566	1.8366	2.9790	2.4762
3000	1.3440	1.5900	4.2815	1.6563	1.8391	1.8903	2.9613	2.4667
4000	1.2753	1.4009	4.2025	1.6166	1.8469	1.9507	2.9496	2.4664
5000	1.2848	1.3879	4.0857	1.5432	1.8513	2.0008	2.9292	2.4652
6000	1.2572	1.3897	3.9393	1.5322	1.8429	2.0591	2.9115	2.4519
7000	1.2306	1.4209	3.7524	1.5303	1.8362	2.0750	2.9094	2.4375
8000	1.2306	1.4863	3.6443	1.5025	1.8363	2.1002	2.9114	2.4381
9000	1.2320	1.5497	3.5247	1.4896	1.8452	2.1416	2.9154	2.4485
10000	1.2320	1.6200	3.3546	1.4675	1.8616	2.1751	2.9263	2.4671
12000	1.2319	1.6508	2.7947	1.4543	1.9361	2.2285	2.9861	2.5030
14000	1.2320	1.6501	2.6164	1.4429	2.0255	2.2497	3.0429	2.5221
16000	1.2320	1.6452	2.4639	1.4295	2.0647	2.2614	3.0618	2.5192
18000	1.2320	1.6447	2.2894	1.4160	2.0842	2.2789	3.0748	2.5015
20000	1.2320	1.6444	2.0641	1.3999	2.0959	2.3044	3.0836	2.4757
40000	1.2320	1.6532	2.0452	1.3442	2.1324	2.3291	3.0896	2.4393
60000	1.2320	1.6649	2.1057	1.3445	2.1348	2.3327	3.0910	2.4383
80000	1.2320	1.6335	2.0914	1.3446	2.1349	2.3330	3.0911	2.4373
100000	1.2320	1.6179	2.0884	1.3446	2.1349	2.3328	3.0911	2.4373
200000	1.2320	1.5084	2.0878	1.3446	2.1349	2.3328	3.0911	2.4373
400000	1.2320	1.5084	2.0878	1.3446	2.1349	2.3328	3.0911	2.4373
600000	1.2320	1.5084	2.0878	1.3446	2.1349	2.3328	3.0911	2.4373
800000	1.2320	1.5084	2.0878	1.3446	2.1349	2.3328	3.0911	2.4373
1000000	1.2320	1.5084	2.0878	1.3446	2.1349	2.3328	3.0911	2.4373

Table 11: Average Euclidean distance value for maximum evaluation for all cases.

### Maximum Optimiser Iteration

Value	Case 1	Case 2	Case 3	Case 4	Case 5	Case 6	Case 7	Case 8
0	1.7773	2.2614	4.6949	1.8935	1.8884	1.8047	2.9794	2.5322
100	1.7171	2.1869	4.6839	1.8401	1.9114	1.8160	3.0140	2.5639
200	1.6826	2.0935	4.6239	1.8064	1.8954	1.8248	3.0140	2.5484
300	1.5415	1.8298	4.5616	1.7891	1.8833	1.8319	3.0091	2.5252
400	1.4995	1.7443	4.4641	1.7326	1.8766	1.8376	2.9998	2.5020
500	1.4347	1.6727	4.4100	1.7057	1.8683	1.8367	2.9790	2.4762
600	1.4213	1.6239	4.3542	1.6831	1.8585	1.8445	2.9680	2.4681
700	1.3760	1.6094	4.3094	1.6651	1.8511	1.8679	2.9613	2.4658
800	1.3112	1.5544	4.2622	1.6491	1.8465	1.9117	2.9605	2.4673
900	1.3030	1.4792	4.2251	1.6389	1.8482	1.9363	2.9570	2.4673
1000	1.2746	1.3994	4.2025	1.6165	1.8522	1.9507	2.9496	2.4664
2000	1.2281	1.4898	3.6443	1.5029	1.8404	2.1002	2.9114	2.4381
3000	1.2320	1.6503	2.7947	1.4543	1.9345	2.2285	2.9861	2.5030
4000	1.2320	1.6450	2.4639	1.4295	2.0601	2.2614	3.0618	2.5192
5000	1.2320	1.6444	2.0641	1.3997	2.0910	2.3044	3.0836	2.4757
6000	1.2320	1.6443	2.0561	1.3660	2.1152	2.3288	3.0851	2.4511
7000	1.2320	1.6461	2.0835	1.3529	2.1238	2.3359	3.0875	2.4424
8000	1.2320	1.6498	2.0858	1.3512	2.1243	2.3369	3.0879	2.4403
9000	1.2320	1.6513	2.0550	1.3465	2.1246	2.3318	3.0879	2.4393
10000	1.2320	1.6533	2.0452	1.3442	2.1265	2.3291	3.0896	2.4393
12000	1.2320	1.6608	2.1064	1.3437	2.1343	2.3314	3.0910	2.4386
14000	1.2320	1.6650	2.1060	1.3443	2.1293	2.3329	3.0910	2.4384
16000	1.2320	1.6661	2.1026	1.3446	2.1294	2.3327	3.0911	2.4381
18000	1.2320	1.6537	2.0977	1.3446	2.1349	2.3328	3.0911	2.4375
20000	1.2320	1.6331	2.0914	1.3446	2.1349	2.3330	3.0911	2.4373
40000	1.2320	1.5186	2.0878	1.3446	2.1349	2.3328	3.0911	2.4373
60000	1.2320	1.5084	2.0878	1.3446	2.1349	2.3328	3.0911	2.4373
80000	1.2320	1.5084	2.0878	1.3446	2.1349	2.3328	3.0911	2.4373
100000	1.2320	1.5084	2.0878	1.3446	2.1349	2.3328	3.0911	2.4373
200000	1.2320	1.5084	2.0878	1.3446	2.1349	2.3328	3.0911	2.4373
400000	1.2320	1.5084	2.0878	1.3446	2.1349	2.3328	3.0911	2.4373
600000	1.2320	1.5084	2.0878	1.3446	2.1349	2.3328	3.0911	2.4373
800000	1.2320	1.5084	2.0878	1.3446	2.1349	2.3328	3.0911	2.4373
1000000	1.2320	1.5084	2.0878	1.3446	2.1349	2.3328	3.0910	2.4373

Table 12: Average Euclidean distance value for maximum optimiser iteration for all cases.

### Minimum Improvement

Value	Case 1	Case 2	Case 3	Case 4	Case 5	Case 6	Case 7	Case 8
1/10	1.7912	2.2659	-	-	-	-	-	-
1/20	1.7758	2.2165	-	-	-	-	-	-
1/30	1.7151	2.1667	-	-	-	-	-	-
1/40	1.2855	2.1493	-	-	-	-	-	-
1/50	1.2723	1.7405	-	-	-	-	-	-
1/60	1.2795	1.7181	-	-	-	-	-	-
1/70	1.2320	1.3898	-	-	-	-	-	-
1/80	1.2320	1.3898	-	-	-	-	-	-
1/90	1.2320	1.6525	-	-	-	-	-	-
1/100	1.2320	1.6501	4.6925	1.8024	1.9089	1.8186	3.0137	2.5521
1/200	1.2320	1.5084	4.6059	1.7326	1.8954	1.8326	3.0117	2.5220
1/300	1.2320	1.5084	4.4451	1.7220	1.8891	1.8362	3.0065	2.4791
1/400	1.2320	1.5084	4.3551	1.6982	1.8805	1.8431	2.9752	2.4724
1/500	1.2320	1.5084	4.2627	1.6961	1.8689	1.8431	2.9717	2.4668
1/600	1.2320	1.5084	4.2412	1.6856	1.8620	1.9300	2.9629	2.4657
1/700	1.2320	1.5084	4.1359	1.6839	1.8675	1.9408	2.9613	2.4663
1/800	1.2320	1.5084	3.9108	1.6579	1.8652	1.9531	2.9597	2.4673
1/900	1.2320	1.5084	3.7041	1.6544	1.8512	2.0525	2.9121	2.4673
1/1000	1.2320	1.5084	3.5856	1.6500	1.8475	2.0593	2.9115	2.4664
1/2000	1.2320	1.5084	2.6260	1.5316	1.8619	2.1577	2.9117	2.5049
1/3000	1.2320	1.5084	2.4473	1.5011	2.0227	2.2217	2.9240	2.5242
1/4000	1.2320	1.5084	2.0858	1.4653	2.0578	2.2264	3.0495	2.4605
1/5000	1.2320	1.5084	2.0818	1.4647	2.0675	2.2521	3.0535	2.4560
1/6000	1.2320	1.5084	2.0843	1.4635	2.0725	2.2540	3.0553	2.4546
1/7000	1.2320	1.5084	2.0852	1.4628	2.0737	2.2543	3.0719	2.4535
1/8000	1.2320	1.5084	2.0854	1.4622	2.0785	2.2612	3.0725	2.4534
1/9000	1.2320	1.5084	2.0936	1.4546	2.0850	2.2668	3.0730	2.4504
1/10000	1.2320	1.5084	2.1124	1.4513	2.0866	2.2696	3.0738	2.4489
1/12000	1.2320	1.5084	2.1140	1.3848	2.0896	2.3086	3.0794	2.4471
1/14000	1.2320	1.5084	2.1143	1.3683	2.0900	2.3125	3.0818	2.4466
1/16000	1.2320	1.5084	2.1148	1.3673	2.1207	2.3128	3.0831	2.4464
1/18000	1.2320	1.5084	2.1148	1.3671	2.1211	2.3293	3.0833	2.4437
1/20000	1.2320	1.5084	2.1143	1.3669	2.1217	2.3306	3.0835	2.4429
1/40000	1.2320	1.5084	2.1259	1.3533	2.1239	2.3299	3.0868	2.4407
1/60000	1.2320	1.5084	2.1257	1.3524	2.1257	2.3292	3.0873	2.4405
1/80000	1.2320	1.5084	2.1219	1.3456	2.1261	2.3303	3.0876	2.4394
1/100000	1.2320	1.5084	2.1219	1.3456	2.1277	2.3307	3.0878	2.4393
1/200000	1.2320	1.5084	2.1020	1.3436	2.1286	2.3321	3.0878	2.4393
1/400000	1.2320	1.5084	2.0982	1.3440	2.1294	2.3327	3.0904	2.4386
1/600000	1.2320	1.5084	2.0978	1.3442	2.1305	2.3326	3.0909	2.4384
1/800000	1.2320	1.5084	2.1082	1.3443	2.1310	2.3327	3.0910	2.4384
1/1000000	1.2320	1.5084	2.0907	1.3443	2.1310	2.3327	3.0910	2.4383
0	1.2320	1.5084	2.0878	1.3446	2.1350	2.3328	3.0910	2.4373

Table 13: Average Euclidean distance value for minimum improvement for all cases.

## Average Euclidean Distance for the Recordings

### Pushing

Camera Recording	Average Euclidean Distance Value divided by Vessel Branches				
	Left	Middle Left	Middle	Middle Right	Right
1	1.226	1.478	1.322	1.694	1.775
2	1.397	1.531	1.594	2.112	1.766
3	1.195	1.600	1.642	empty	1.766
4	1.409	1.769	1.589	1.971	1.757
5	empty	1.700	1.667	1.780	1.807
6	1.210	1.685	1.660	1.885	1.799
7	1.161	1.286	1.623	1.803	1.445
8	1.679	1.603	1.607	1.938	1.565

Table 14: Average Euclidean distance value for the recordings, while pushing the catheter.

### Pulling

Camera Recording	Average Euclidean Distance Value divided by Vessel Branches				
	Left	Middle Left	Middle	Middle Right	Right
1	1.093	1.251	1.064	1.567	1.279
2	1.134	1.315	1.213	1.889	1.036
3	1.081	1.326	1.198	empty	1.090
4	1.106	1.244	1.049	1.614	1.268
5	empty	1.306	1.299	1.753	1.080
6	1.121	1.292	1.268	1.696	1.097
7	1.130	1.276	1.450	1.594	1.034
8	1.153	1.141	1.592	1.878	1.087

Table 15: Average Euclidean distance value for the recordings, while pulling the catheter.



## Statutory Declaration

### Eidesstattliche Erklärung

Ich versichere hiermit, dass ich die vorliegende Master Thesis mit dem o.a. formulierten Thema ohne fremde Hilfe selbstständig verfasst und nur die angegebenen Quellen und Hilfsmittel verwendet habe.

Wörtlich oder dem Sinn nach aus anderen Werken entnommene Stellen sind unter der Angabe der Quellen kenntlich gemacht.

---